Article

Gait Analysis for a Tiltrotor: The Dynamic Invertible Gait

Zhe Shen * and Takeshi Tsuchiya

Department of Aeronautics and Astronautics, The University of Tokyo, Tokyo 113-8654, Japan;
tsuchiya@mail.ecc.u-tokyo.ac.jp
* Correspondence: zheshen@g.ecc.u-tokyo.ac.jp

Abstract: A conventional feedback-linearization-based controller, when applied to a tiltrotor (eight inputs), results in extensive changes in tilting angles, which are not expected in practice. To solve this problem, we introduce the novel concept of "UAV gait" to restrict the tilting angles. The gait plan was initially used to solve the control problems in quadruped (four-legged) robots. Applying this approach, accompanied by feedback linearization, to a tiltrotor may give rise to the well-known non-invertible problem in the decoupling matrix. In this study, we explored invertible gait in a tiltrotor, and applied feedback linearization to stabilize the attitude and the altitude. The conditions necessary to achieve a full-rank decoupling matrix were deduced and simplified to near-zero roll and zero pitch. This paper proposes several invertible gaits to conduct an attitude–altitude control test. The accepted gaits within the region of interest were visualized. The simulation was conducted in Simulink, MATLAB. The results show promising responses in stabilizing attitude and altitude.

1. Introduction

In the past decade, tiltrotors have attracted great interest. Tiltrotors are a novel type of quadrotor [1–8], wherein the axes of the propellers tilt, imparting the ability to change the direction of each thrust. Typical control methods to stabilize a tiltrotor include LQR and PID [9–11], backstepping and sliding mode [12–16], feedback linearization [17–23], optimal control [24–26], adaptive control [27,28], etc. Feedback linearization [29–31] explicitly decouples the nonlinear parts, and enables one to utilize the over-actuated properties. This approach is not only effective for a standard tiltrotor, but also for a tiltrotor with predetermined tilting angles [32].

Given the benefits of feedback linearization, we have achieved capabilities such as tracking with a rapid response for sophisticated references [17,18,22]. However, several potential risks may hinder the applications of this technique. One of these is saturation restriction. This limit refers to the upper bound of a given motor and the non-negative bound of the thrust; negative thrust is usually not acceptable in applications. Some research has focused on avoiding either of the above bounds [33–36]. Although hitting a boundary does not necessarily result in instability, the corresponding stability criteria for these cases can be hard to trace or generalize [37–39].

Another typical issue of feedback linearization when applied in over-actuated systems is the so-called "State Drift" phenomenon, as defined in [40]; the state or input may drift as the simulation continues. In [1,22], the authors defined the optimal control conditions to avert this problem. The extra requirements restrict the freedom of the inputs to some extent. Unfortunately, relevant stability proof has not been provided. An alternative method to avoid state drift is to reduce the number of inputs by predefining some of them [40]. This method is inspired by gait plan, which is widely adopted in quadruped (four-legged) robots [41–45].

The number of inputs (the magnitude of each thrust and the direction of each thrust) of the tiltrotor in this research was eight at most. The number of degrees of freedom was

six (attitude and position). The current feedback-linearization-based control strategies used to stabilize this tiltrotor are categorized into two groups.

One seeks to manipulate all eight inputs so that the tiltrotor becomes an over-actuated system with the potential to simultaneously maneuver in all degrees of freedom. The other sacrifices the number of inputs to make it equal to the number of degrees of freedom; a typical means of achieving this is to make the tilting angles of the thrusts at the opposite arms equal.

However, both strategies lead to unrealistic changes in tilting angles. The tilting angles undergo large changes during flight [1,22]; some of these are unexpectedly fast. These requirements are hardly practical; a reasonable tilting angle should be within a small range and not extend beyond a certain period (2π).

In this research, we prohibited changes in tilting angles during our flight and analyzed each combination of four tilting angles to find those wherein feedback linearization was applicable (i.e., the decoupling matrix was invertible). This means that the number of inputs was four in this research. Furthermore, the accepted region for designing the gait was explored in an attitude–altitude stabilization test.

We compared the control result by completing the same task but with the other controller, which fully utilized all the inputs (over-actuated) of the same tiltrotor with identical parameters.

The rest of this paper is structured as follows. Section 2 introduces the dynamics of the tiltrotor. Then, the developed feedback-linearization-based controller is presented in Section 3. The necessary conditions for an applicable gait are analyzed in Section 4. In the simulation presented in Section 5, the attitude and the altitude of the tiltrotor were stabilized by the controller proposed in Section 3. Section 6 shows the results and the sufficient conditions for an applicable gait in the region of interest. The conclusions and discussions are addressed in Section 7.

2. Dynamics of the Tiltrotor

A tiltrotor is a type of modified quadrotor whose directions of thrust are able to change [1–7]. Figure 1 illustrates a tiltrotor. Here, the direction of each thrust is shown in the corresponding yellow plane. For details of the kinematics, [1,2,4,5,7] are recommended.
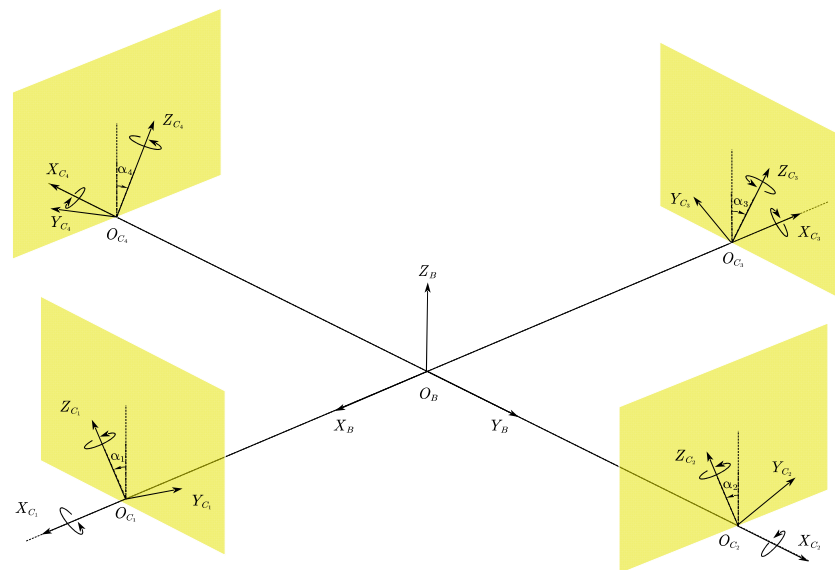

Figure 1. Sketch of the tiltrotor.

Among the quadrotor dynamics discussed in previous research, the widely accepted model from [1,2,7,22] is constructed by separately analyzing each part (body frame, tilting

motor frames, and propeller frames) using Newton's Law. The controller was developed based on simplified dynamics via Equations (1)–(5).

The position $P = \begin{bmatrix} X & Y & Z \end{bmatrix}^T$ is given by:

$$\ddot{P} = \begin{bmatrix} 0 \\ 0 \\ -g \end{bmatrix} + \frac{1}{m} \cdot {}^W R \cdot F(\alpha) \cdot \begin{bmatrix} \varpi_1 \cdot |\varpi_1| \\ \varpi_2 \cdot |\varpi_2| \\ \varpi_3 \cdot |\varpi_3| \\ \varpi_4 \cdot |\varpi_4| \end{bmatrix}$$

$$\triangleq \begin{bmatrix} 0 \\ 0 \\ -g \end{bmatrix} + \frac{1}{m} \cdot {}^W R \cdot F(\alpha) \cdot w \tag{1}$$

where m is the total mass, g is the gravitational acceleration, and ϖ_i, $(i = 1, 2, 3, 4)$ is the angular velocity of the propeller ($\varpi_{1,3} < 0$, $\varpi_{2,4} > 0$) with respect to the propeller-fixed frame, $w = \begin{bmatrix} w_1 & w_2 & w_3 & w_4 \end{bmatrix}^T$. $w_i = \varpi_i \cdot |\varpi_i|$, m is the mass of the tilt-rotor. Rotor 1 and Rotor 3 were assumed to rotate clockwise. Rotor 2 and Rotor 4 were assumed to rotate counter-clockwise. ${}^W R$ is the rotational matrix [46] between the inertial frame and the body-fixed frame (Equation (2)):

$$^W R = \begin{bmatrix} c\theta \cdot c\psi & s\phi \cdot s\theta \cdot c\psi - c\phi \cdot s\psi & c\phi \cdot s\theta \cdot c\psi + s\phi \cdot s\psi \\ c\theta \cdot s\psi & s\phi \cdot s\theta \cdot s\psi + c\phi \cdot c\psi & c\phi \cdot s\theta \cdot s\psi - s\phi \cdot c\psi \\ -s\theta & s\phi \cdot c\theta & c\phi \cdot c\theta \end{bmatrix}, \tag{2}$$

where $s\Lambda = \sin(\Lambda)$ and $c\Lambda = \cos(\Lambda)$. ϕ, θ, and ψ are the roll angle, pitch angle, and yaw angle, respectively. The tilting angles $\alpha = \begin{bmatrix} \alpha_1 & \alpha_2 & \alpha_3 & \alpha_4 \end{bmatrix}$. The positive directions of the tilting angles are defined in Figure 1. $F(\alpha)$ is defined as:

$$F(\alpha) = \begin{bmatrix} 0 & K_f \cdot s2 & 0 & -K_f \cdot s4 \\ K_f \cdot s1 & 0 & -K_f \cdot s3 & 0 \\ -K_f \cdot c1 & K_f \cdot c2 & -K_f \cdot c3 & K_f \cdot c4 \end{bmatrix} \tag{3}$$

where $si = \sin(\alpha_i)$, $ci = \cos(\alpha_i)$, and $(i = 1, 2, 3, 4)$. K_f ($8.048 \times 10^{-6} \text{N} \cdot \text{s}^2/\text{rad}^2$) is the coefficient of the thrust.

The angular velocity of the body with respect to its own frame, $\omega_B = \begin{bmatrix} p & q & r \end{bmatrix}^T$, is governed by Newton–Euler Formula as:

$$\dot{\omega}_B = I_B^{-1} \cdot \tau(\alpha) \cdot w \tag{4}$$

where I_B is the matrix of moments of inertia, K_m ($2.423 \times 10^{-7} \text{N} \cdot \text{m} \cdot \text{s}^2/\text{rad}^2$) is the coefficient of the drag, and L is the length of the arm:

$$\tau(\alpha) = \begin{bmatrix} 0 & L \cdot K_f \cdot c2 - K_m \cdot s2 & 0 & -L \cdot K_f \cdot c4 + K_m \cdot s4 \\ L \cdot K_f \cdot c1 + K_m \cdot s1 & 0 & -L \cdot K_f \cdot c3 - K_m \cdot s3 & 0 \\ L \cdot K_f \cdot s1 - K_m \cdot c1 & -L \cdot K_f \cdot s2 - K_m \cdot c2 & L \cdot K_f \cdot s3 - K_m \cdot c3 & -L \cdot K_f \cdot s4 - K_m \cdot c4 \end{bmatrix}. \tag{5}$$

Thus far, we have determined the dynamics of a tiltrotor. There are several remarks we can make.

Firstly, the tilting angles ($\alpha_1, \alpha_2, \alpha_3, \alpha_4$) are predetermined before controlling. This indicates that they are constant during flight, i.e.,:

$$\dot{\alpha}_i \equiv 0, i = 1, 2, 3, 4. \tag{6}$$

In this research, we will determine the proper tilting angles required to support our flight.

Secondly, the relationship [47–49] between the angular velocity of the body, ω_B, and the attitude rotation matrix ($^W R$) is given by:

$$^W \dot{R} = {}^W R \cdot \hat{\omega}_B \tag{7}$$

where "^" is the hat operation used to produce the skew matrix, and $^W \dot{R}$ represents the derivative of rotation matrix.

Our simulator was built based on Equations (1)–(7).

In the controller design process, we approximated the relationship between the angular velocity of the body, ω_B, and the attitude angle, (ϕ, θ, ψ), by:

$$\begin{bmatrix} \dot{\phi} \\ \dot{\theta} \\ \dot{\psi} \end{bmatrix} = \omega_B. \tag{8}$$

Instead of further exploiting Equation (7), the controller was designed based on Equations (1)–(6) and (8).

The parameters of this tiltrotor are as follows: $m = 0.429$ kg, $L = 0.1785$ m, $g = 9.8$ N/kg, and $I_B = \text{diag}\left(\left[2.24 \times 10^{-3}, 2.99 \times 10^{-3}, 4.80 \times 10^{-3}\right]\right)$ kg·m^2.

3. Feedback Linearization and Control

The control scenario consisted of two sections. Firstly, the nonlinear dynamics were dynamically inverted by feedback linearization. Secondly, the linearized system was stabilized based on a third-order PD controller. The rest of this section introduces these strategies.

3.1. Feedback Linearization

The first step in feedback linearization is to select the output. In this research, we chose attitude–altitude, described in Equation (9), as our output, because the choice of position–yaw may introduce a further singular zone [50,51]:

$$\begin{bmatrix} y_1 \\ y_2 \\ y_3 \\ y_4 \end{bmatrix} = \begin{bmatrix} \phi \\ \theta \\ \psi \\ Z \end{bmatrix}. \tag{9}$$

Calculating the second derivative of Equation (9) yields:

$$\begin{bmatrix} \ddot{y}_1 \\ \ddot{y}_2 \\ \ddot{y}_3 \\ \ddot{y}_4 \end{bmatrix} = \begin{bmatrix} 0 \\ 0 \\ 0 \\ -g \end{bmatrix} + \begin{bmatrix} I_B^{-1} \cdot \tau(\alpha) \\ \begin{bmatrix} 0 & 0 & 1 \end{bmatrix} \cdot \frac{K_f}{m} \cdot {}^W R \cdot F(\alpha) \end{bmatrix}^{4 \times 4} \cdot w. \tag{10}$$

Notably, we derive Equation (11) if $\varpi_{1,3} < 0$, $\varpi_{2,4} > 0$:

$$(\varpi_i \cdot |\varpi_i|)' = 2 \cdot \dot{\varpi}_i \cdot |\varpi_i|. \tag{11}$$

Differentiating Equation (10) yields:

$$\begin{bmatrix} \dddot{y}_1 \\ \dddot{y}_2 \\ \dddot{y}_3 \\ \dddot{y}_4 \end{bmatrix} = \begin{bmatrix} I_B{}^{-1} \cdot \tau(\alpha) \\ \begin{bmatrix} 0 & 0 & 1 \end{bmatrix} \cdot \frac{K_f}{m} \cdot {}^W R \cdot F(\alpha) \cdot 2 \cdot \begin{bmatrix} |\omega_1| & & & \\ & |\omega_2| & & \\ & & |\omega_3| & \\ & & & |\omega_4| \end{bmatrix} \end{bmatrix}^{4 \times 4} \cdot \begin{bmatrix} \dot{\omega}_1 \\ \dot{\omega}_2 \\ \dot{\omega}_3 \\ \dot{\omega}_4 \end{bmatrix}$$

$$+ \begin{bmatrix} 0 & 0 & 1 \end{bmatrix} \cdot \frac{K_f}{m} \cdot {}^W R \cdot \hat{\omega}_B \cdot F(\alpha) \cdot w \cdot \begin{bmatrix} 0 \\ 0 \\ 0 \\ 1 \end{bmatrix} \tag{12}$$

$$\triangleq \overline{\Delta} \cdot \begin{bmatrix} \dot{\omega}_1 \\ \dot{\omega}_2 \\ \dot{\omega}_3 \\ \dot{\omega}_4 \end{bmatrix} + Ma$$

where $\overline{\Delta}$ is called the decoupling matrix [32], and $\begin{bmatrix} \dot{\omega}_1 & \dot{\omega}_2 & \dot{\omega}_3 & \dot{\omega}_4 \end{bmatrix}^T \triangleq U$ is the new input vector.

From Equation (12), we may derive the decoupled relationship in Equation (13), which is compatible with the controller design process:

$$\begin{bmatrix} \dot{\omega}_1 \\ \dot{\omega}_2 \\ \dot{\omega}_3 \\ \dot{\omega}_4 \end{bmatrix} = \overline{\Delta}^{-1} \cdot \left(\begin{bmatrix} \dddot{y}_{1d} \\ \dddot{y}_{2d} \\ \dddot{y}_{3d} \\ \dddot{y}_{4d} \end{bmatrix} - Ma \right). \tag{13}$$

Obviously, the necessary condition for receiving Equation (13) is that the decoupling matrix ($\overline{\Delta}$) is invertible. Section 4 deepens this discussion.

Once solving Equation (13), the controller may be applied to this linearized system. In this research, we deployed third-order PD controllers.

3.2. Third-Order PD Controllers

We designed the third-order PD controllers as:

$$\begin{bmatrix} \dddot{y}_{1d} \\ \dddot{y}_{2d} \\ \dddot{y}_{3d} \end{bmatrix} = \begin{bmatrix} \dddot{y}_{1r} \\ \dddot{y}_{2r} \\ \dddot{y}_{3r} \end{bmatrix} + K_{P1}{}^{3 \times 3} \cdot \left(\begin{bmatrix} \ddot{y}_{1r} \\ \ddot{y}_{2r} \\ \ddot{y}_{3r} \end{bmatrix} - \begin{bmatrix} \ddot{y}_1 \\ \ddot{y}_2 \\ \ddot{y}_3 \end{bmatrix} \right) + K_{P2}{}^{3 \times 3} \cdot \left(\begin{bmatrix} \dot{y}_{1r} \\ \dot{y}_{2r} \\ \dot{y}_{3r} \end{bmatrix} - \begin{bmatrix} \dot{y}_1 \\ \dot{y}_2 \\ \dot{y}_3 \end{bmatrix} \right) + K_{P3}{}^{3 \times 3} \cdot \left(\begin{bmatrix} y_{1r} \\ y_{2r} \\ y_{3r} \end{bmatrix} - \begin{bmatrix} y_1 \\ y_2 \\ y_3 \end{bmatrix} \right), \tag{14}$$

$$\dddot{y}_{4d} = \dddot{y}_{4r} + K_{PZ_1} \cdot (\ddot{y}_{4r} - \ddot{y}_4) + K_{PZ_2} \cdot (\dot{y}_{4r} - \dot{y}_4) + K_{PZ_3} \cdot (y_{4r} - y_4), \tag{15}$$

where K_{Pi} ($i = 1, 2, 3$) is the three-by-three diagonal control coefficient matrix, K_{PZ_i} ($i = 1, 2, 3$) is the control coefficient (scalar), y_j ($j = 1, 2, 3, 4$) is the state, and y_{jr} ($j = 1, 2, 3, 4$) is the reference.

The control parameters in this section are specified as follows: $K_{P1} = K_{P2} = K_{P3} = \text{diag}([1, 1, 1])$, $K_{PZ_1} = 10$, $K_{PZ_2} = 5$, and $K_{PZ_3} = 10$.

4. Applicable Gait (Necessary Conditions)

As discussed, the necessary condition for applying this control is that the decoupling matrix ($\overline{\Delta}$) is invertible. In this section, we find the equivalent conditions to derive an invertible decoupling matrix.

Notice the relationship:

$$\overline{\Delta} \sim \begin{bmatrix} \tau(\alpha) \\ \begin{bmatrix} 0 & 0 & 1 \end{bmatrix} \cdot {}^W R \cdot F(\alpha) \end{bmatrix} \tag{16}$$

where "$A \sim B$" indicates that Matrix A is equivalent to Matrix B. Two matrices are called equivalent if, and only if, there exist invertible matrices P and Q, so that $A = P \cdot B \cdot Q$.

The following propositions and proofs are specifically applicable only to the tiltrotor with our chosen control parameters and coefficients.

Proposition 1. *The decoupling matrix is invertible if, and only if:*

$$
\begin{aligned}
&1.000 \cdot c1 \cdot c2 \cdot c3 \cdot s4 \cdot s\theta - 1.000 \cdot c1 \cdot s2 \cdot c3 \cdot c4 \cdot s\theta \\
&- 2.880 \cdot c1 \cdot c2 \cdot s3 \cdot s4 \cdot s\theta + 2.880 \cdot c1 \cdot s2 \cdot s3 \cdot c4 \cdot s\theta \\
&- 2.880 \cdot s1 \cdot c2 \cdot c3 \cdot s4 \cdot s\theta + 2.880 \cdot s1 \cdot s2 \cdot c3 \cdot c4 \cdot s\theta \\
&- 1.000 \cdot s1 \cdot c2 \cdot s3 \cdot s4 \cdot s\theta + 1.000 \cdot s1 \cdot s2 \cdot s3 \cdot c4 \cdot s\theta \\
&+ 4.000 \cdot c1 \cdot c2 \cdot c3 \cdot c4 \cdot c\phi \cdot c\theta + 5.592 \cdot c1 \cdot c2 \cdot c3 \cdot s4 \\
&\cdot c\phi \cdot c\theta - 5.592 \cdot c1 \cdot c2 \cdot s3 \cdot c4 \cdot c\phi \cdot c\theta + 5.592 \cdot c1 \cdot s2 \\
&\cdot c3 \cdot c4 \cdot c\phi \cdot c\theta - 5.592 \cdot s1 \cdot c2 \cdot c3 \cdot c4 \cdot c\phi \cdot c\theta + 1.000 \\
&\cdot c1 \cdot c2 \cdot s3 \cdot c4 \cdot s\phi \cdot c\theta + 0.9716 \cdot c1 \cdot c2 \cdot s3 \cdot s4 \cdot c\phi \cdot c\theta \\
&- 2.000 \cdot c1 \cdot s2 \cdot c3 \cdot s4 \cdot c\phi \cdot c\theta + 0.9716 \cdot c1 \cdot s2 \cdot s3 \cdot c4 \\
&\cdot c\phi \cdot c\theta - 1.000 \cdot s1 \cdot c2 \cdot c3 \cdot c4 \cdot s\phi \cdot c\theta + 0.9716 \cdot s1 \cdot c2 \\
&\cdot c3 \cdot s4 \cdot c\phi \cdot c\theta - 2.000 \cdot s1 \cdot c2 \cdot s3 \cdot c4 \cdot c\phi \cdot c\theta + 0.9716 \\
&\cdot s1 \cdot s2 \cdot c3 \cdot c4 \cdot c\phi \cdot c\theta + 2.880 \cdot c1 \cdot c2 \cdot s3 \cdot s4 \cdot s\phi \cdot c\theta \\
&+ 2.880 \cdot c1 \cdot s2 \cdot s3 \cdot c4 \cdot s\phi \cdot c\theta - 0.1687 \cdot c1 \cdot s2 \cdot s3 \cdot s4 \cdot \\
&c\phi \cdot c\theta - 2.880 \cdot s1 \cdot c2 \cdot c3 \cdot s4 \cdot s\phi \cdot c\theta + 0.1687 \cdot s1 \cdot c2 \\
&\cdot s3 \cdot s4 \cdot c\phi \cdot c\theta - 2.880 \cdot s1 \cdot s2 \cdot c3 \cdot c4 \cdot s\phi \cdot c\theta - 0.1687 \\
&\cdot s1 \cdot s2 \cdot c3 \cdot s4 \cdot c\phi \cdot c\theta + 0.1687 \cdot s1 \cdot s2 \cdot s3 \cdot c4 \cdot c\phi \cdot c\theta \\
&- 1.000 \cdot c1 \cdot s2 \cdot s3 \cdot s4 \cdot s\phi \cdot c\theta + 1.000 \cdot s1 \cdot s2 \cdot c3 \cdot s4 \\
&\cdot s\phi \cdot c\theta \\
&\neq 0
\end{aligned}
\tag{17}
$$

Proof of Proposition 1. *Expanding the second matrix in Equation (16) yields:*

$$
\overline{\Delta} \sim
\begin{bmatrix}
0 & L \cdot K_f \cdot c2 - K_m \cdot s2 & 0 & -L \cdot K_f \cdot c4 + K_m \cdot s4 \\
L \cdot K_f \cdot c1 + K_m \cdot s1 & 0 & -L \cdot K_f \cdot c3 - K_m \cdot s3 & 0 \\
L \cdot K_f \cdot s1 - K_m \cdot c1 & -L \cdot K_f \cdot s2 - K_m \cdot c2 & L \cdot K_f \cdot s3 - K_m \cdot c3 & -L \cdot K_f \cdot s4 - K_m \cdot c4 \\
c\theta \cdot s\phi \cdot s1 - c\theta \cdot c\phi \cdot c1 & -s\theta \cdot s2 + c\theta \cdot c\phi \cdot c2 & -c\theta \cdot s\phi \cdot s3 - c\theta \cdot c\phi \cdot c3 & s\theta \cdot s4 + c\theta \cdot c\phi \cdot c4
\end{bmatrix}.
\tag{18}
$$

Calculating the determinant of the second matrix in Equation (18) yields Condition (17). □

Proposition 2. *When the roll angle and pitch angle of the tiltrotor are close to zero, the decoupling matrix is invertible if, and only if:*

$$
\begin{aligned}
&4.000 \cdot c1 \cdot c2 \cdot c3 \cdot c4 + 5.592 \\
&\cdot (+c1 \cdot c2 \cdot c3 \cdot s4 - c1 \cdot c2 \cdot s3 \cdot c4 + c1 \cdot s2 \cdot c3 \cdot c4 - s1 \cdot c2 \cdot c3 \cdot c4) \\
&+ 0.9716 \\
&\cdot (+c1 \cdot c2 \cdot s3 \cdot s4 + c1 \cdot s2 \cdot s3 \cdot c4 + s1 \cdot c2 \cdot c3 \cdot s4 + s1 \cdot s2 \cdot c3 \cdot c4) \\
&+ 2.000 \cdot (-c1 \cdot s2 \cdot c3 \cdot s4 - s1 \cdot c2 \cdot s3 \cdot c4) + 0.1687 \\
&\cdot (-c1 \cdot s2 \cdot s3 \cdot s4 + s1 \cdot c2 \cdot s3 \cdot s4 - s1 \cdot s2 \cdot c3 \cdot s4 + s1 \cdot s2 \cdot s3 \cdot c4) \\
&\neq 0.
\end{aligned}
\tag{19}
$$

Proof of Proposition 2. *Make the assumptions in Equations (20) and (21):*

$$
\theta = 0.
\tag{20}
$$

$$
\phi = 0.
\tag{21}
$$

Substituting Equations (20) and (21) into Condition (17) yields Condition (19). □

Remark 1. *One may believe that Equation (18) would be an applicable gait-selecting zone, where any combination of* $(\alpha_1, \alpha_2, \alpha_3, \alpha_4)$ *satisfying Proposition 1 would lead to a stable result. Unfortunately, this is not always true, because the proven Proposition only guarantees the invertibility of the decoupling matrix. Hitting the non-negative angular velocity bound for* ω_i *can result in instability. Obviously, neither Proposition 1 nor Proposition 2 rules out this situation. This is why we call the Propositions the "necessary" conditions for an applicable gait. The sufficient condition within the range of interest is presented in the simulation in* Sections 5 *and* 6.

Remark 2. *Notably, Condition (17) not only restricts the gait* $(\alpha_1, \alpha_2, \alpha_3, \alpha_4)$, *but also rules out some attitudes* (ϕ, θ); *a specific gait can be driven to violate Condition (17) while steering to some specific attitudes. In actuality, a similar attitude-based condition means the failure makes the decoupling matrix invertible in* [50], *hindering further applications in feedback linearization (position–yaw output) before modification. This is because roll and pitch are not directly controlled via the position–yaw output choice. However, the adverse effect of this property is weakened in our research. The output choice (attitude–altitude) enables the tiltrotor to directly steer the attitude. Thus, roll angle and pitch angle can be relatively arbitrarily assigned. Steering the attitude away from the region violating Condition (17) is consequently made possible by this controller.*

5. Attitude–Altitude Stabilization Test

The conditions in Section 4 are necessary in achieving the applicable gait. The sufficient conditions are explored empirically in this section.

To reduce the complexity, the preliminary step was to restrict the gait to some extent and find the gait region of interest. The next step was to determine the exploration direction of the candidate gaits. The final step was to conduct the simulation for each gait along the exploring direction.

5.1. Restricted Gait Region

The simulation was conducted at near-zero roll angle and pitch angle ($\phi = 0, \theta = 0$). Thus, the following analysis is based on Condition (19) rather than on Condition (17).

Although Condition (19) includes no information about the roll angle and pitch angle, there are still four parameters in the gait ($\alpha_1, \alpha_2, \alpha_3, \alpha_4$) to be determined, which is a complicated issue. Here, we simplify the gait first.

Instead of exploring the entire space of ($\alpha_1, \alpha_2, \alpha_3, \alpha_4$), we explore four gaits with one of the following restrictions in each gait: $\alpha_1 = \alpha_3$, $\alpha_1 = \frac{1}{2} \cdot \alpha_3$, $\alpha_1 = -\alpha_3$, and $\alpha_1 = -\frac{1}{2} \cdot \alpha_3$.

5.1.1. Case 1 (Equal)

This section demonstrates the result for some cases satisfying $\alpha_1 = \alpha_3$. Specifically, $\alpha_1 = \alpha_3 = -0.15, -0.075, 0, 0.075, 0.15$. Figure 2 plots the left side of Condition (19). The result is five surfaces about (α_2, α_4). Intercepting the surfaces in Figure 2 by the zero plane (Determinant $= 0$) yields Figure 3. Figure 3 plots (α_2, α_4), violating Condition (19).

5.1.2. Case 2 (Half)

This section presents the results for some cases satisfying $\alpha_1 = \frac{1}{2} \cdot \alpha_3$. Specifically, $\alpha_1 = \frac{1}{2} \cdot \alpha_3 = -0.2, -0.1, 0, 0.1, 0.2$. Figure 4 plots the left side of Condition (19). The result is five surfaces about (α_2, α_4). Intercepting the surfaces in Figure 4 by the zero plane (Determinant $= 0$) yields Figure 5. Figure 5 plots the (α_2, α_4) violating Condition (19).
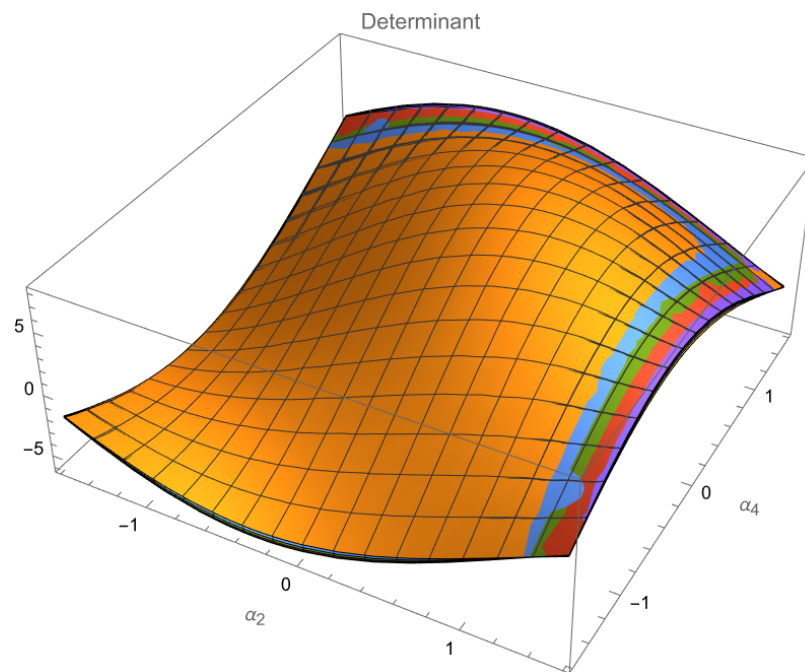
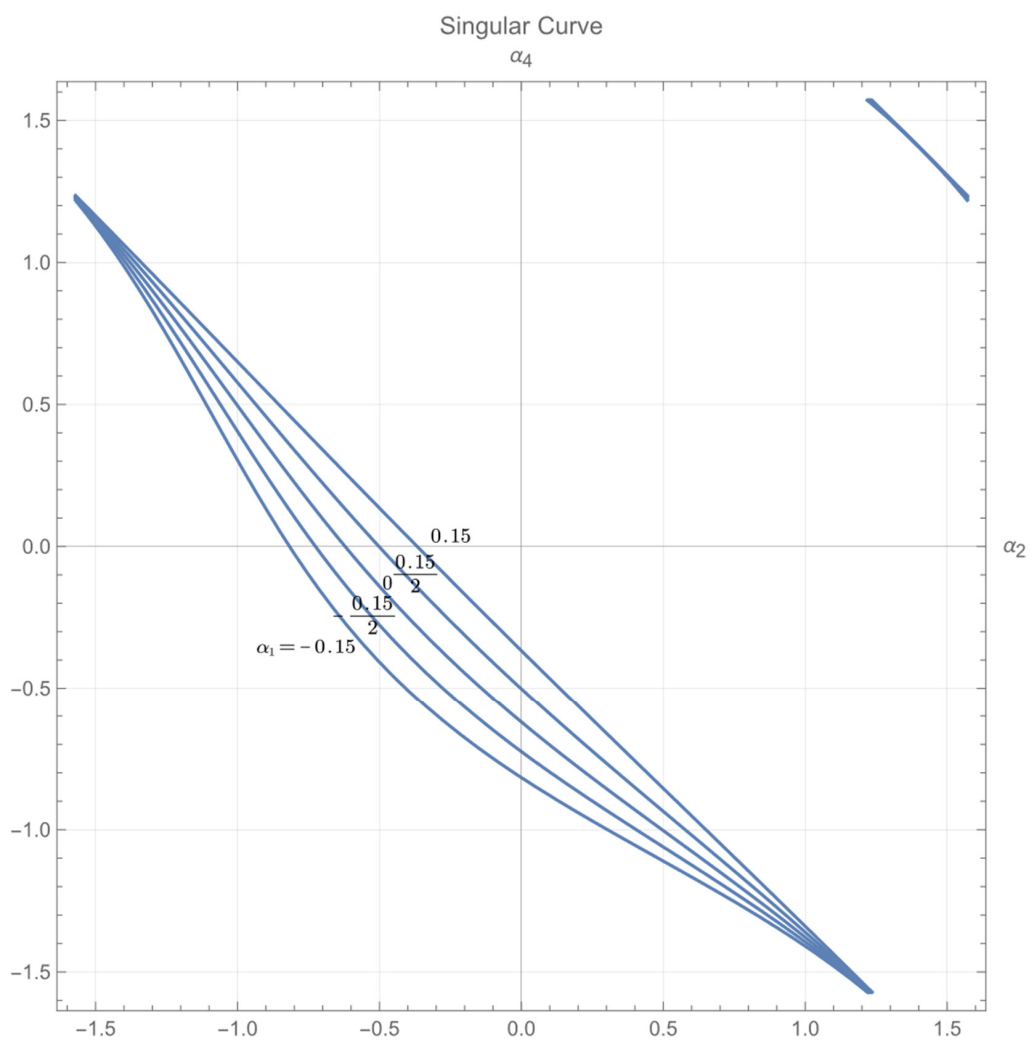**Figure 2.** Surfaces of the determinant ($\alpha_1 = \alpha_3$).

Figure 3. (α_2, α_4) violating Condition (19) ($\alpha_1 = \alpha_3$).
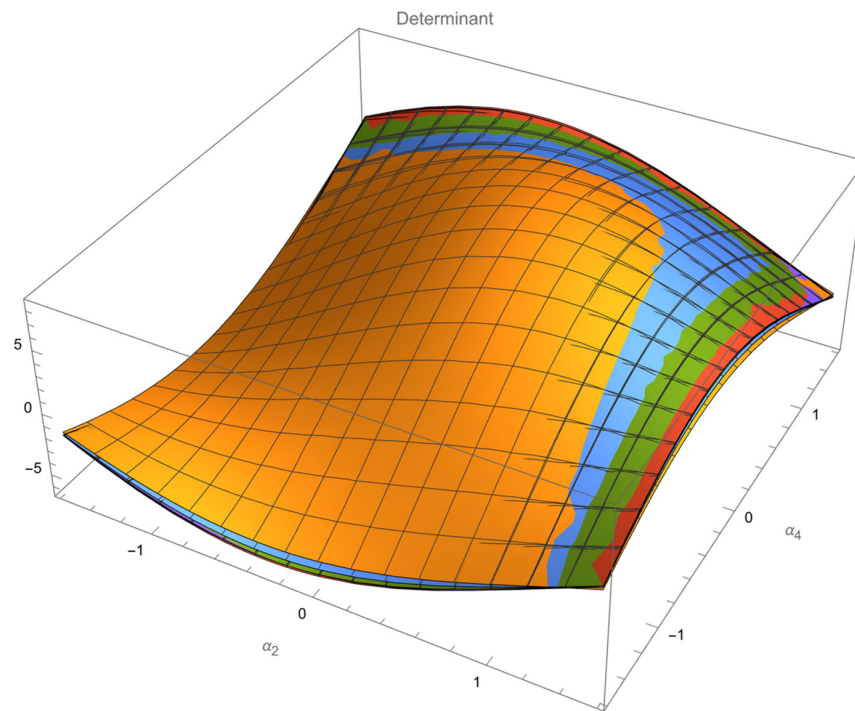
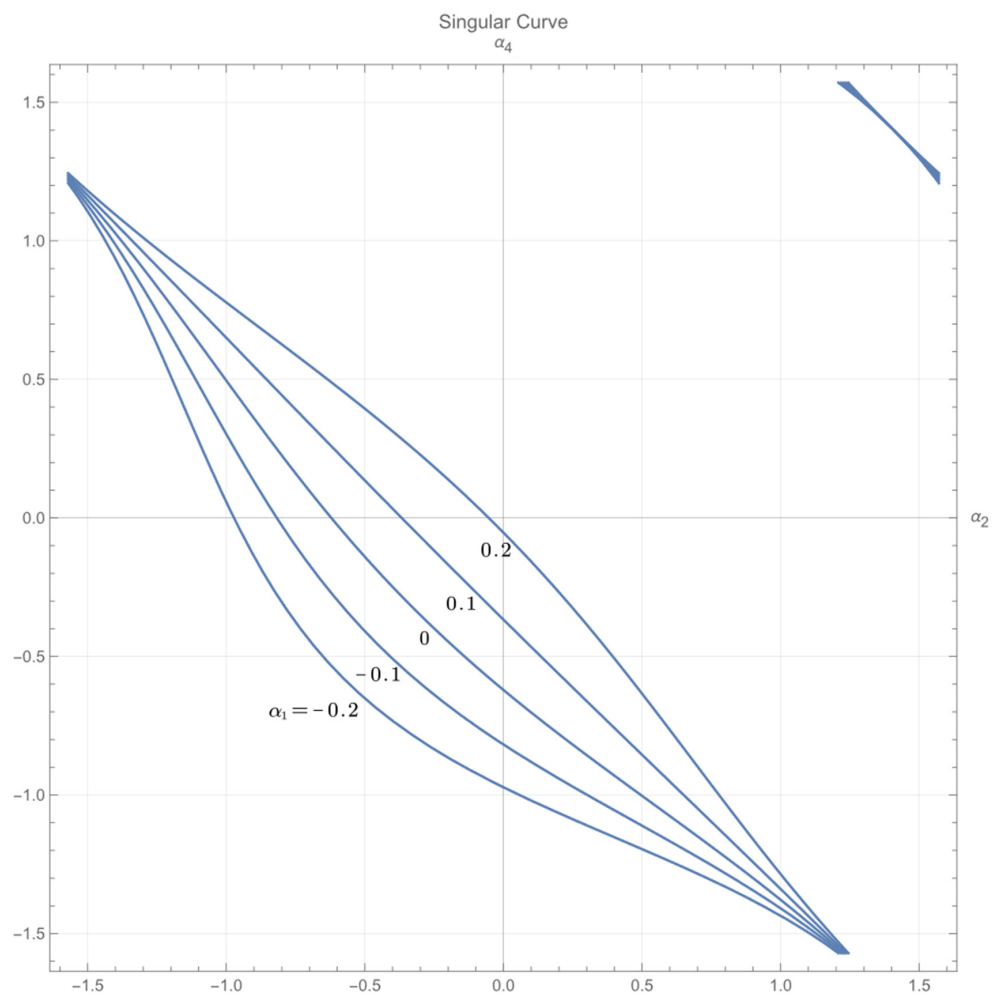**Figure 4.** Surfaces of the determinant ($\alpha_1 = \frac{1}{2} \cdot \alpha_3$).

Figure 5. (α_2, α_4) violating Condition (19) ($\alpha_1 = \frac{1}{2} \cdot \alpha_3$).

5.1.3. Case 3 (Negative)

This section presents the results for some cases satisfying $\alpha_1 = -\alpha_3$. Specifically, $\alpha_1 = -\alpha_3 = -1.4, -0.7, 0, 0.7, 1.4$. Figure 6 plots the left side of Condition (19). The result is five surfaces about (α_2, α_4). Intercepting the surfaces in Figure 6 by the zero plane (Determinant $= 0$) yields Figure 7. Figure 7 plots (α_2, α_4), violating Condition (19).

5.1.4. Case 4 (Negative Half)

This section presents the result for some cases satisfying $\alpha_1 = -\frac{1}{2} \cdot \alpha_3$. Specifically, $\alpha_1 = -\frac{1}{2} \cdot \alpha_3 = -0.3, -0.15, 0, 0.15, 0.3$. Figure 8 plots the left side of Condition (19). The result is five surfaces about (α_2, α_4). Intercepting the surfaces in Figure 8 by the zero plane (Determinant $= 0$) yields Figure 9. Figure 9 plots (α_2, α_4), violating Condition (19).

5.2. *Interested Gait Region and Direction of Exploration*

Notably, choosing the gait of (α_2, α_4) on the relevant curve in Figures 3, 5, 7 and 9 is strictly prohibited. The decline in the relevant curve indicates the violation of Condition (19). It is also worth mentioning that the tiltrotor becomes the conventional quadrotor in terms of gait, satisfying $(\alpha_1, \alpha_2, \alpha_3, \alpha_4) = (0, 0, 0, 0)$. Our gait analysis includes this special case.

Another point worth mentioning is the continuous requirement of gait switching. For example, switching from $(\alpha_2, \alpha_4) = (1, 1)$ to $(\alpha_2, \alpha_4) = (-1, -1)$ is determined to violate Condition (19) for any of the cases shown in Figures 3, 5, 7 and 9. This is because the relevant switching process will cross the curve, which should be prohibited.

Given these concerns, we only choose part of the region containing $(\alpha_2, \alpha_4) = (0, 0)$ as the gait region of interest.

5.2.1. Interested Gait Region

It can be concluded from the green region in Figures 10–13 that any (α_2, α_4) located within or on the edge of the triangular zone defined in (22) for each case in Section 5.1 will not violate Condition (19).

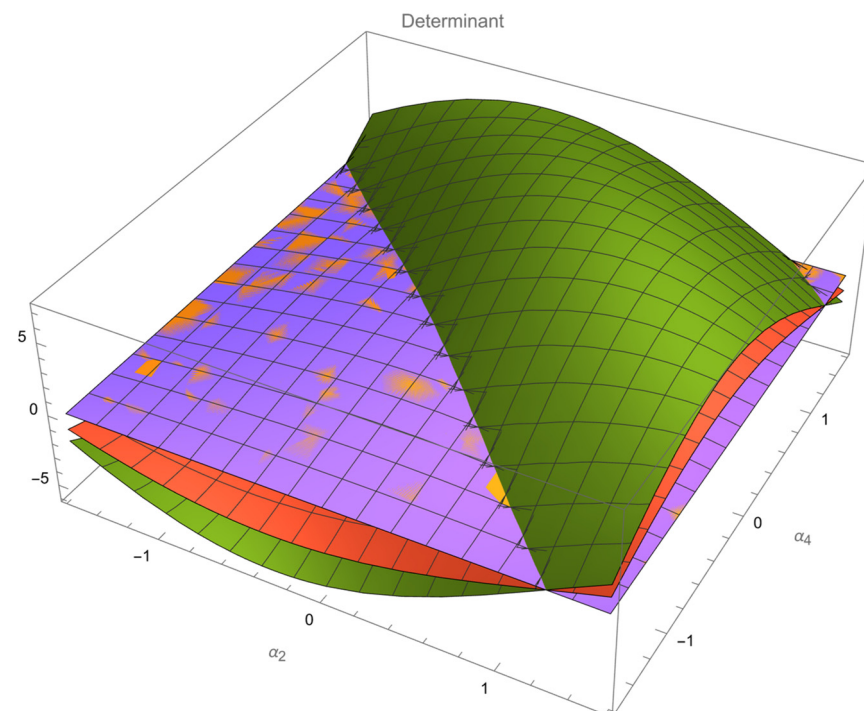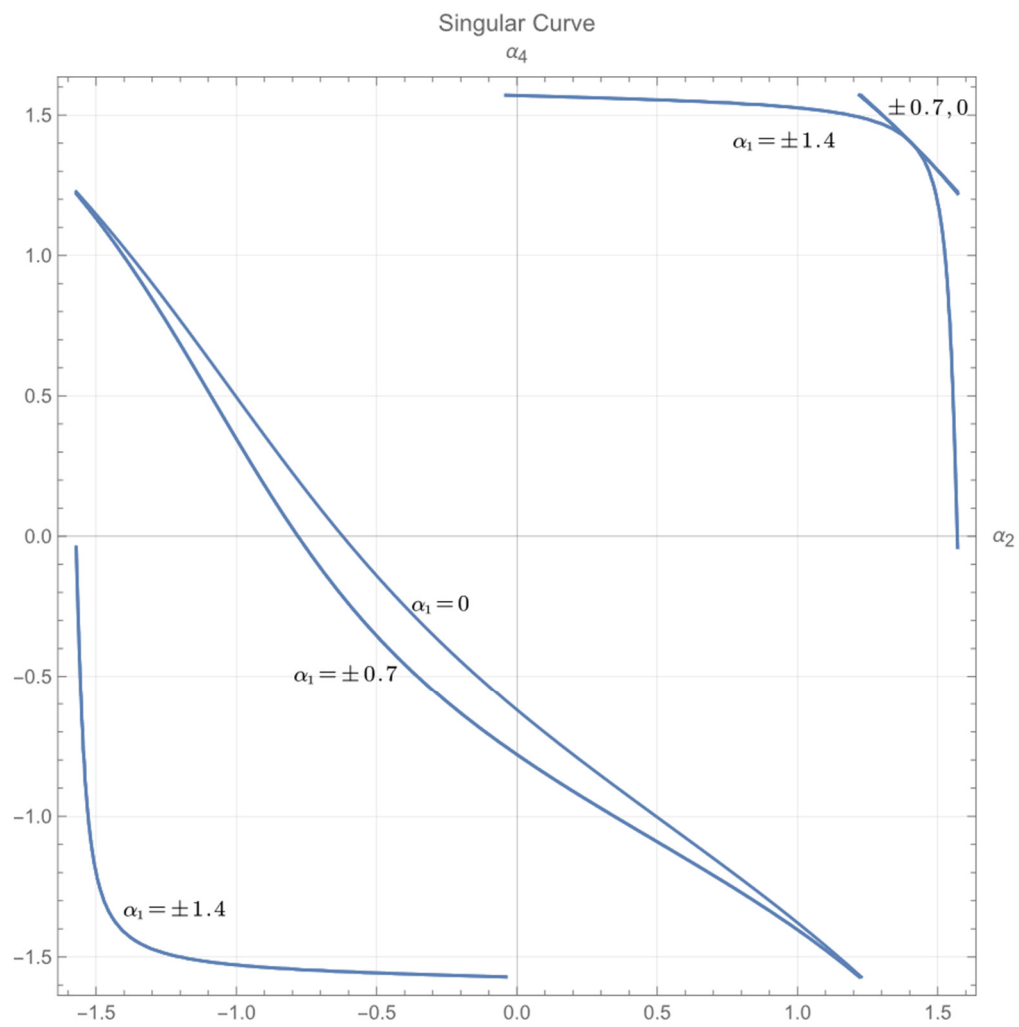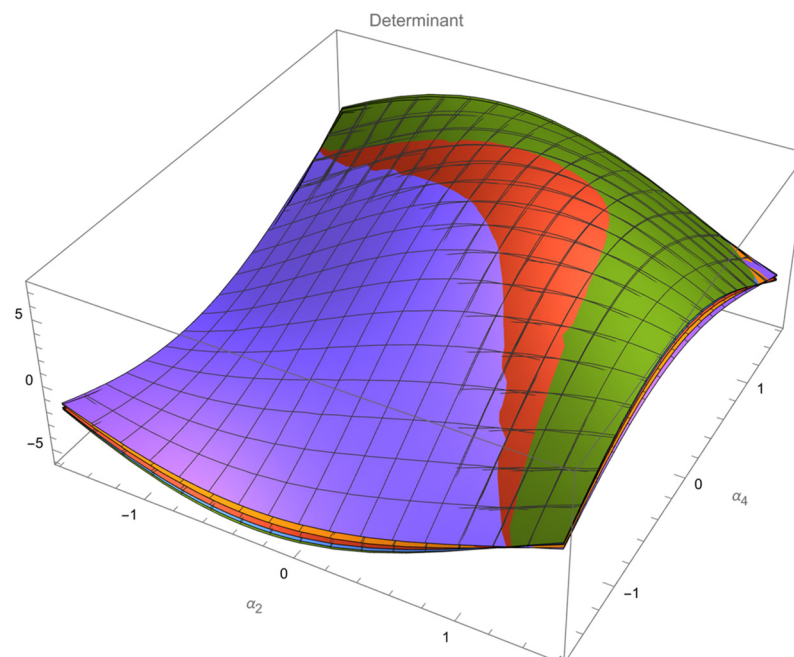**Figure 6.** Surfaces of the determinant $(\alpha_1 = -\alpha_3)$.

Figure 7. (α_2, α_4) violating Condition (19) ($\alpha = -\alpha_3$).

Figure 8. Surfaces of the determinant ($\alpha_1 = -\frac{1}{2} \cdot \alpha_3$).

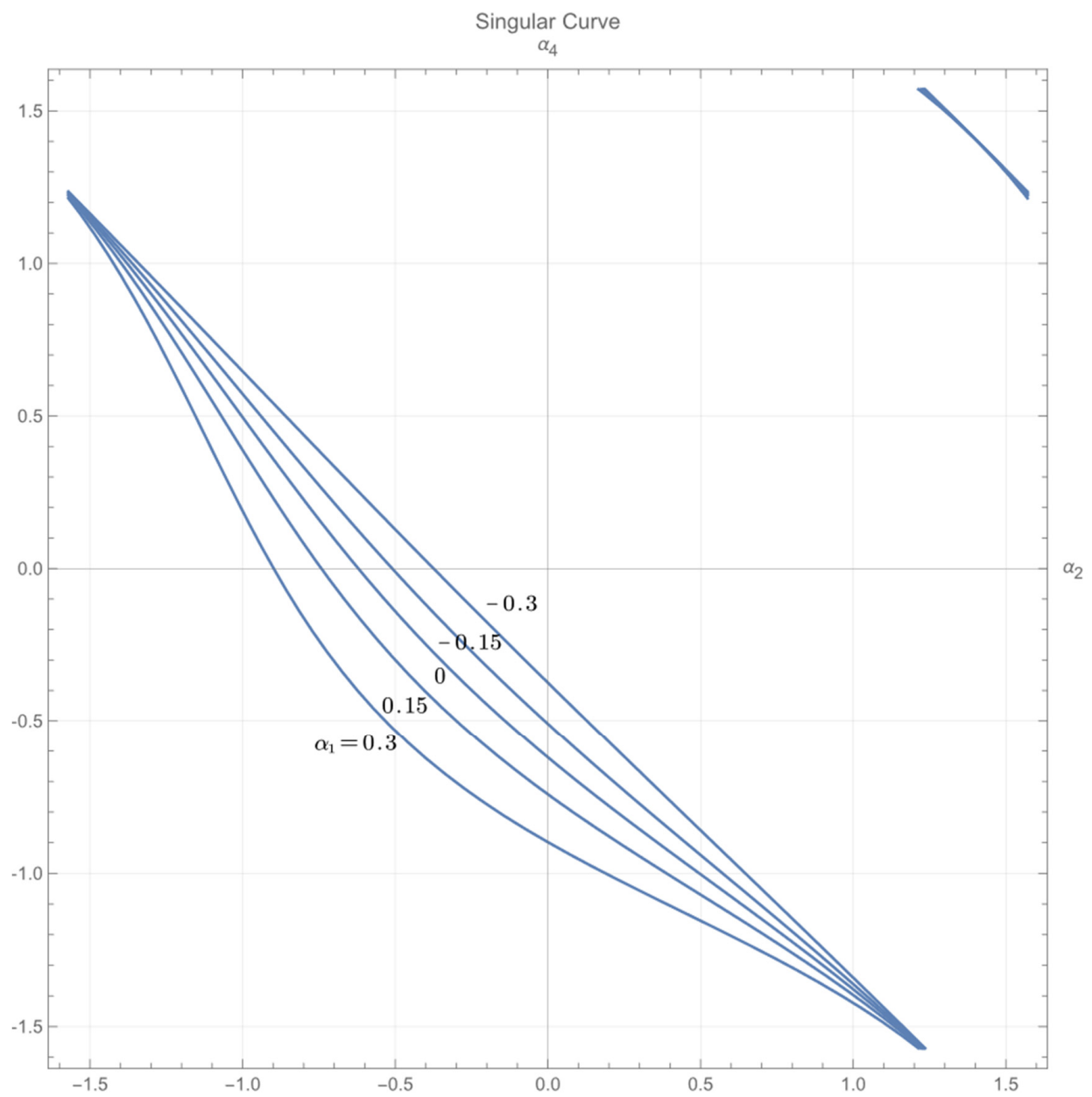**Figure 9.** (α_2, α_4) violating Condition (19) $(\alpha_1 = -\frac{1}{2} \cdot \alpha_3)$.
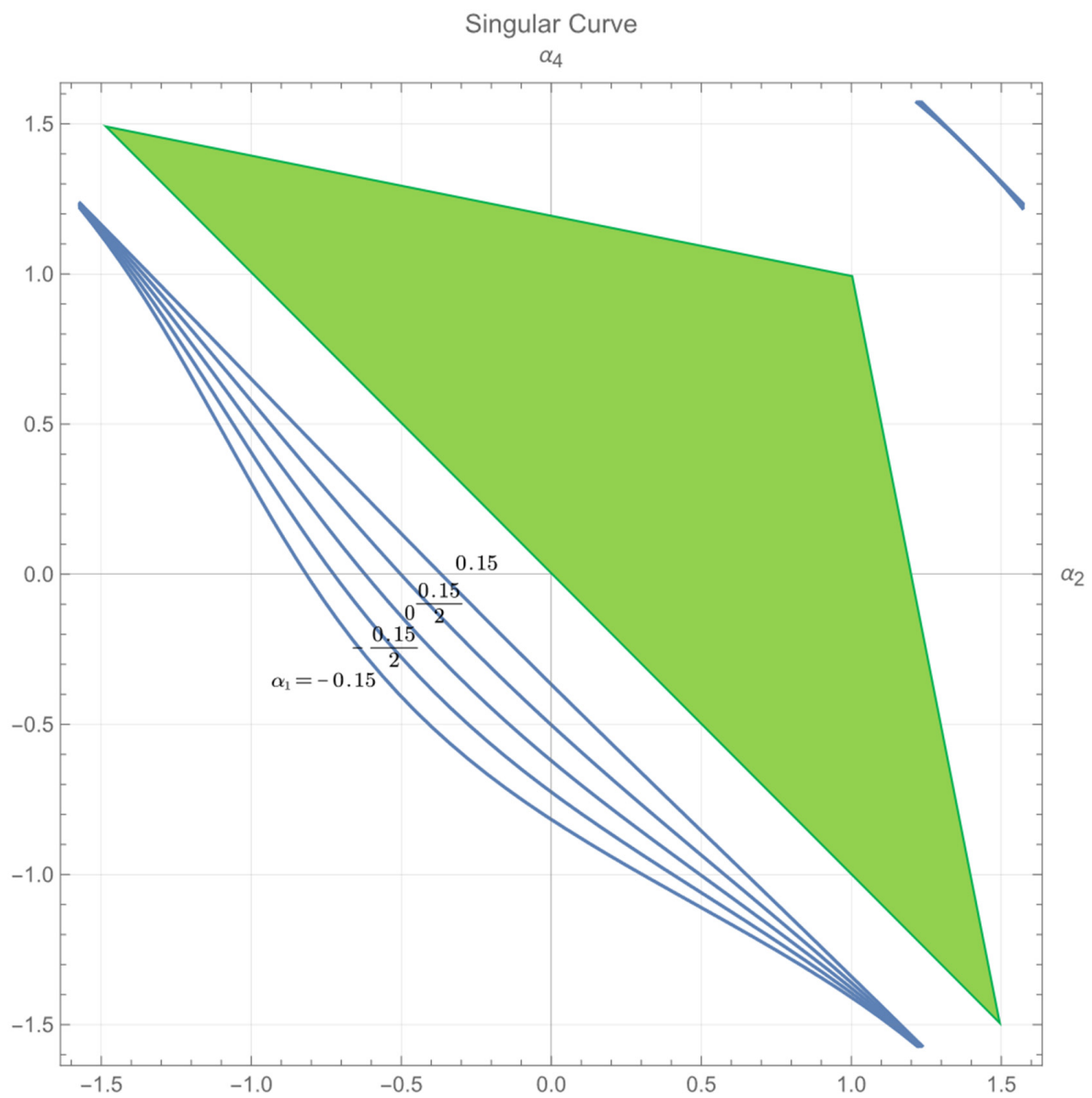
Figure 10. The invertible triangular region of interest ($\alpha_1 = \alpha_3$).
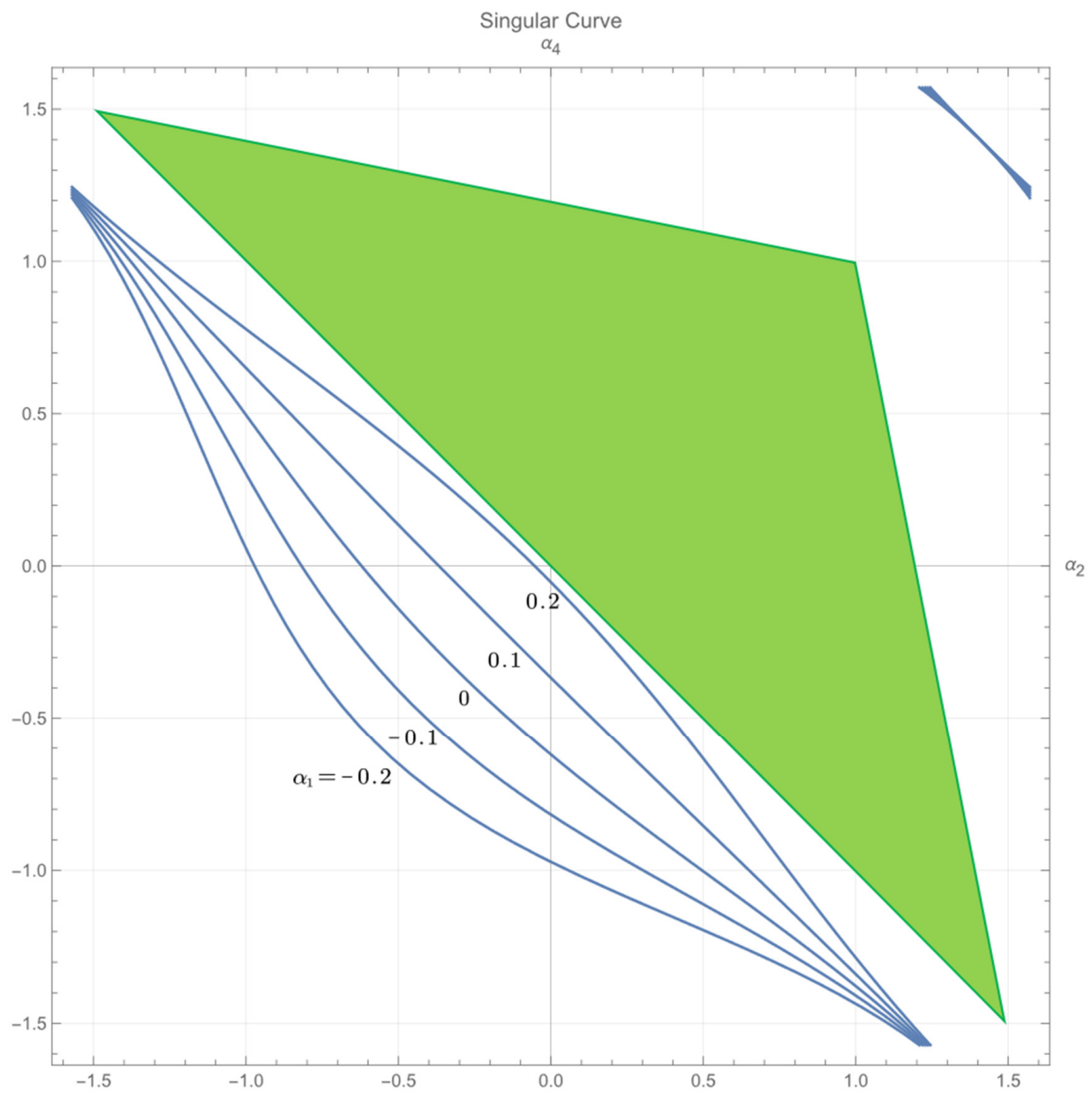
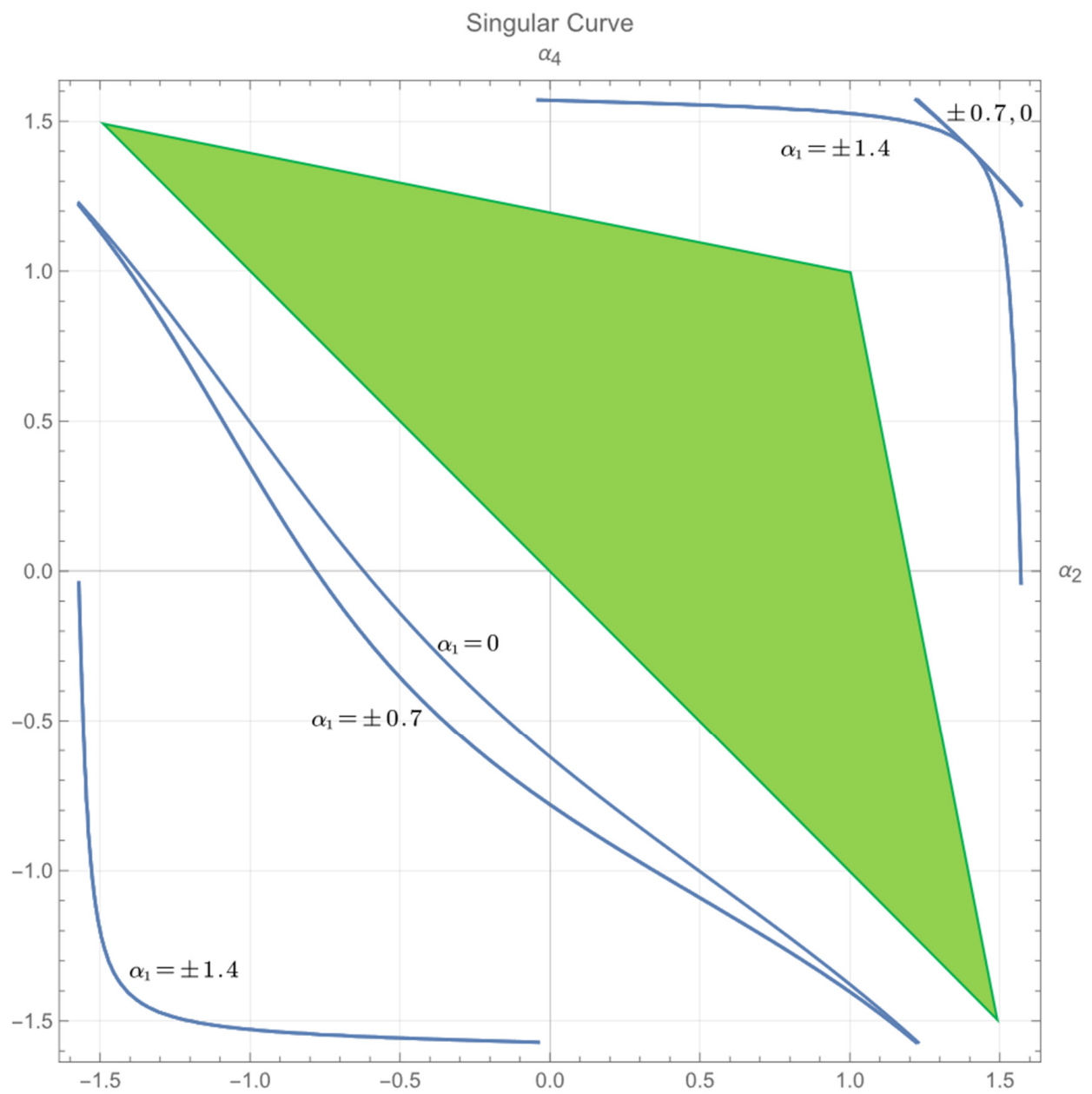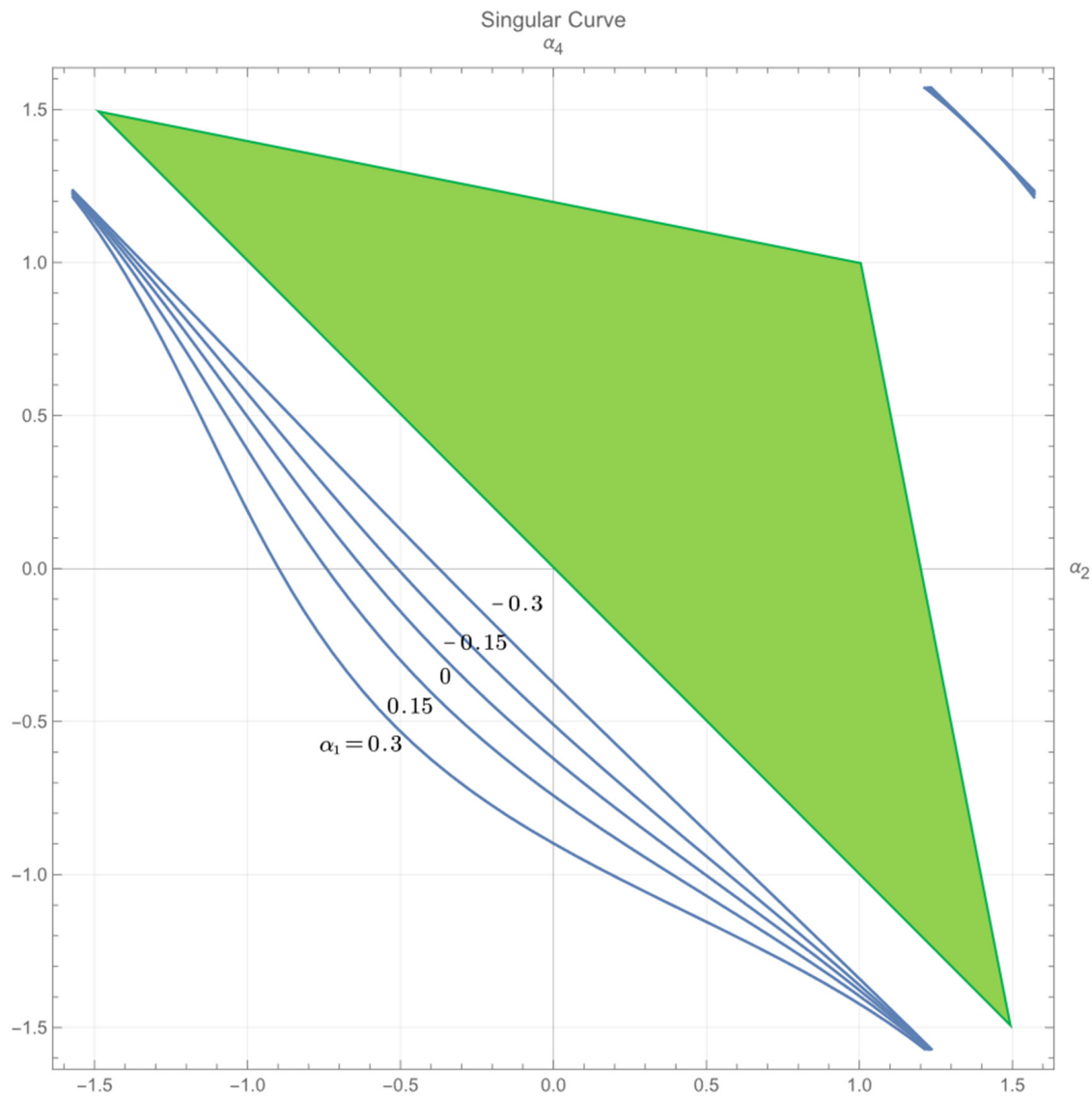**Figure 11.** The invertible triangular region of interest ($\alpha_1 = \frac{1}{2} \cdot \alpha_3$).

Figure 12. The invertible triangular region of interest ($\alpha_1 = -\alpha_3$).

Figure 13. The invertible triangular region of interest ($\alpha_1 = -\frac{1}{2} \cdot \alpha_3$).

The rest of the paper focuses on the gait $(\alpha_1, \alpha_2, \alpha_3, \alpha_4)$, satisfying:

$$\text{Region within or on } \Delta MUV \text{ governed by } U(-1.5, 1.5), \ V(1.5, -1.5), \ M(1, 1). \tag{22}$$

These gaits naturally satisfy the necessary condition given in Proposition 2. Section 5.2.2 outlines the direction of exploration for the simulation identifying the sufficient conditions of stability within the zone in (22).

5.2.2. Direction of Exploration

Exploring the entire space defined in (22) is not necessary or achievable. Thus, we explore parts of this region based on the definition of the directions of exploration in (23)–(25):

$$\alpha_4 = -\alpha_2, \alpha_2 \in \left[-\frac{3}{2}, 0 \right]. \tag{23}$$

$$\alpha_4 = -\alpha_2, \alpha_2 \in \left[0, \frac{3}{2} \right]. \tag{24}$$

$$\alpha_4 = \alpha_2, \alpha_2 \in [0, 1]. \tag{25}$$

The exploration in each direction given in (23)–(25) starts from $|\alpha_2| = 0$. With the predetermined α_1 and α_3, the exploration ends at a critical α_{2M}, defined in (26):

$$\forall \alpha_2 \; satisfying \; |\alpha_2| \leqslant |\alpha_{2C}|, (\alpha_1, \alpha_2, \alpha_3, \alpha_4) \Rightarrow stable,$$
$$\exists \alpha_2 \; satisfying \; |\alpha_2| > |\alpha_{2C}|, (\alpha_1, \alpha_2, \alpha_3, \alpha_4) \Rightarrow unstable. \tag{26}$$
$$\alpha_{2M} = \text{sign}(\alpha_2) \cdot \max(|\alpha_{2C}|).$$

The expected output is the three gaits $(\alpha_1, \alpha_2, \alpha_3, \alpha_4)$ corresponding to the three α_{2M} along the directions given in (23)–(25).

5.3. Attitude–Altitude Control

Feedback linearization relies on the choice of output. In this research, the selected output was the attitude–altitude vector; we focus on only controlling the attitude and altitude. Notably, this control scheme can also be used to reach a desired position with a conventional quadrotor [52], which can be regarded as the special case in our tiltrotor, where $(\alpha_1, \alpha_2, \alpha_3, \alpha_4) = (0,0,0,0)$. However, position control in a tiltrotor was not the primary interest of this study.

In this simulation, the tiltrotor was expected to achieve attitude–altitude self-adjustment.

The initial attitude angles of the tiltrotor were assigned as $\phi_i = 0$, $\theta_i = 0$, and $\phi_i = 0$. The initial angular velocity vector of the tiltrotor with respect to the body-fixed frame was $\omega_B = [0,0,0]^T$. The initial position vector was $[0,0,0]^T$. The initial velocity vector was $[0,0,0]^T$.

The input vector is the derivative of each value of angular velocity of the propeller $\left[\dot{\omega}_1, \dot{\omega}_2, \dot{\omega}_3, \dot{\omega}_4 \right]^T$; therefore, assigning an initial velocity for each propeller was necessary. The absolute value of each initial angular velocity was 300 (rad). Notably, these angular velocities are not sufficient to compensate for the effect of gravity, even for the case $(\alpha_1, \alpha_2, \alpha_3, \alpha_4) = (0,0,0,0)$.

The reference was a four-dimensional attitude–altitude vector, $[\phi_r, \theta_r, \psi_r, Z_r]^T$. To maintain zero attitude and zero height, the designed reference was $[0,0,0,0]^T$. Based on the control parameters set in Section 3 and each gait designed in Section 5, we recorded the gaits giving stable results.

6. Results

This section presents the results of the tests in the previous section. Section 6.1 shows the histories of the attitude, altitude, and angular velocities during flights of two typical gaits. Section 6.2 displays the admissible gaits. These are the results of the work described in Section 5.2.2. Section 6.3 presents the results for the same task completed with another control strategy, which utilized all the inputs (over-actuated) on the same tiltrotor with identical parameters.

6.1. Flight History

Section 6.1 presents the results from two gaits. Gait 1: $(\alpha_1, \alpha_2, \alpha_3, \alpha_4) = (-0.1, 0.1, -0.2, 0.1)$. Gait 2: $(\alpha_1, \alpha_2, \alpha_3, \alpha_4) = (-0.15, -0.1, 0.3, -0.1)$.

6.1.1. Gait 1

For the gait $(\alpha_1, \alpha_2, \alpha_3, \alpha_4) = (-0.1, 0.1, -0.2, 0.1)$, the attitude history, altitude history and angular velocities history of the propellers are plotted in Figures 14–16, respectively.
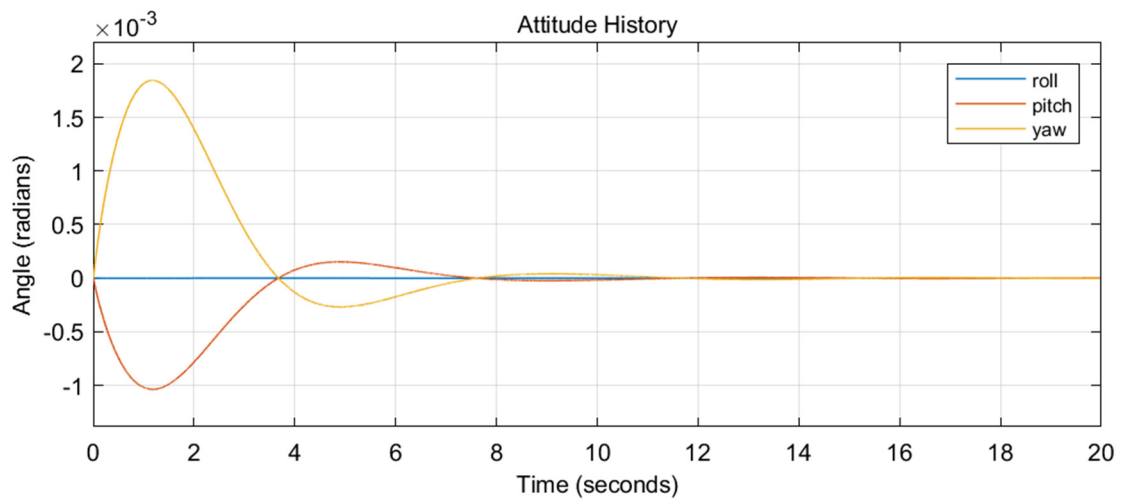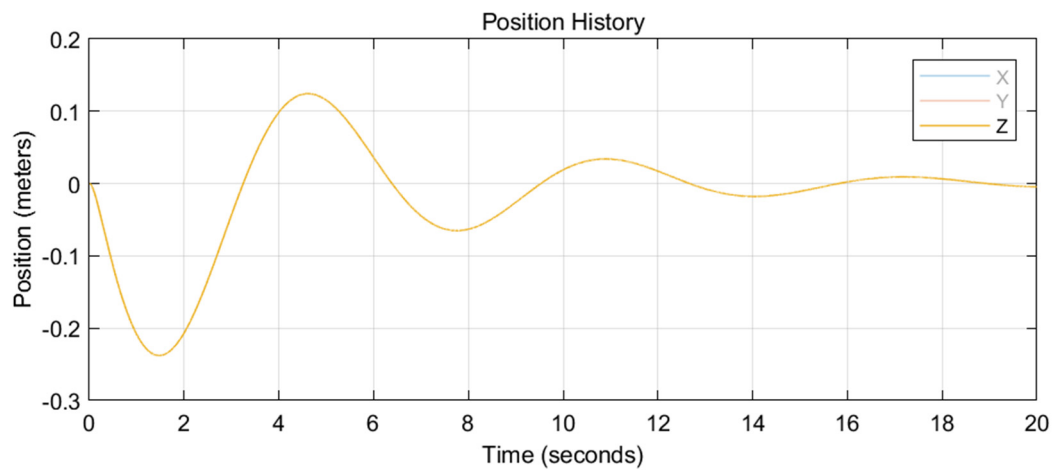
Figure 14. Attitude history of Gait 1.

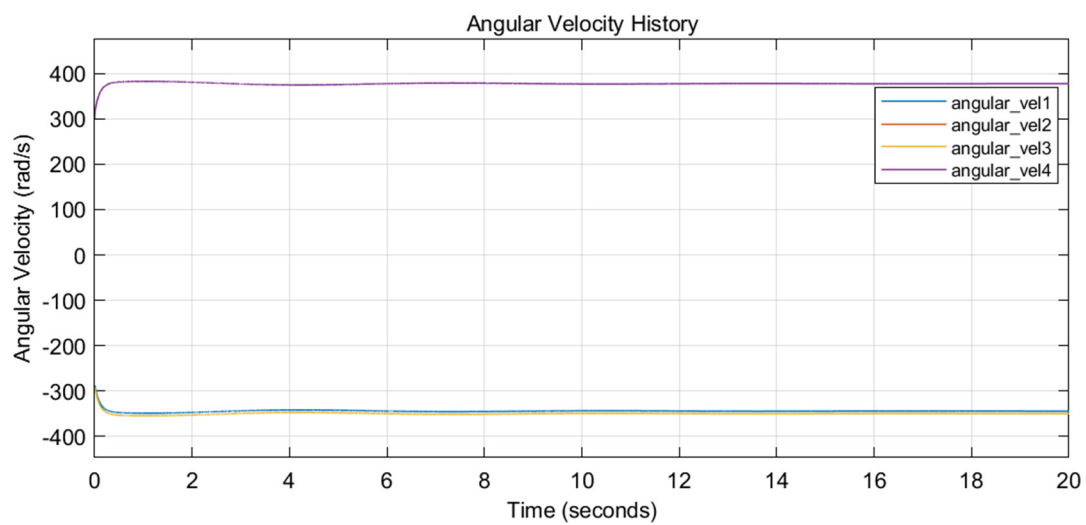**Figure 15.** Altitude history of Gait 1.

Figure 16. Angular velocity history of Gait 1.

Notably, none of the angular velocities touched 0, which guarantees the invertibility of the decoupling matrix in (12).

6.1.2. Gait 2

For the gait $(\alpha_1, \alpha_2, \alpha_3, \alpha_4) = (-0.15, -0.1, 0.3, -0.1)$, the attitude history, altitude history and angular velocities history of the propellers are plotted in Figures 17–19, respectively.

Similarly, none of the angular velocities touched 0.

The specific gaits leading to stable control results for different (α_1, α_3) are detailed in Figures 20–23.
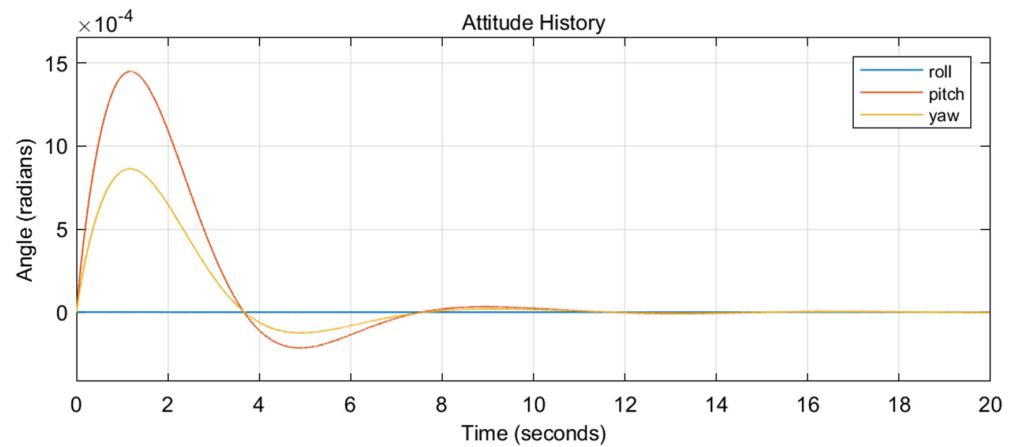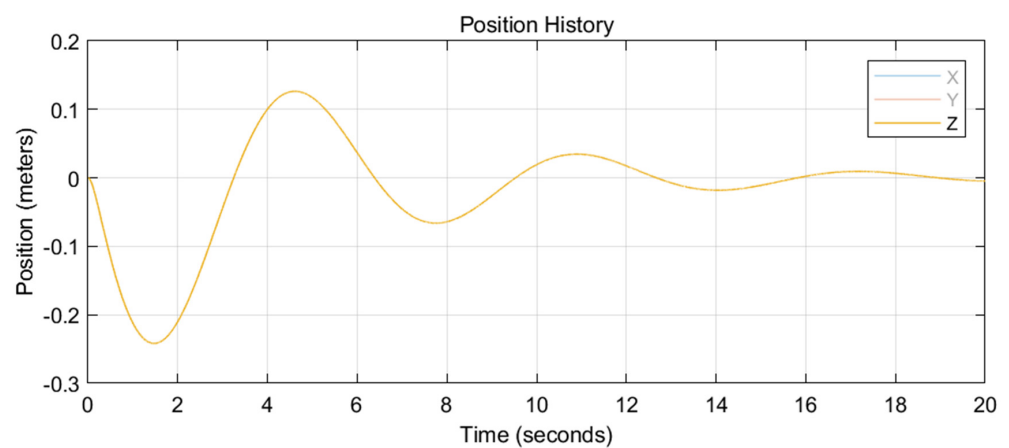

Figure 17. Attitude history of Gait 2.

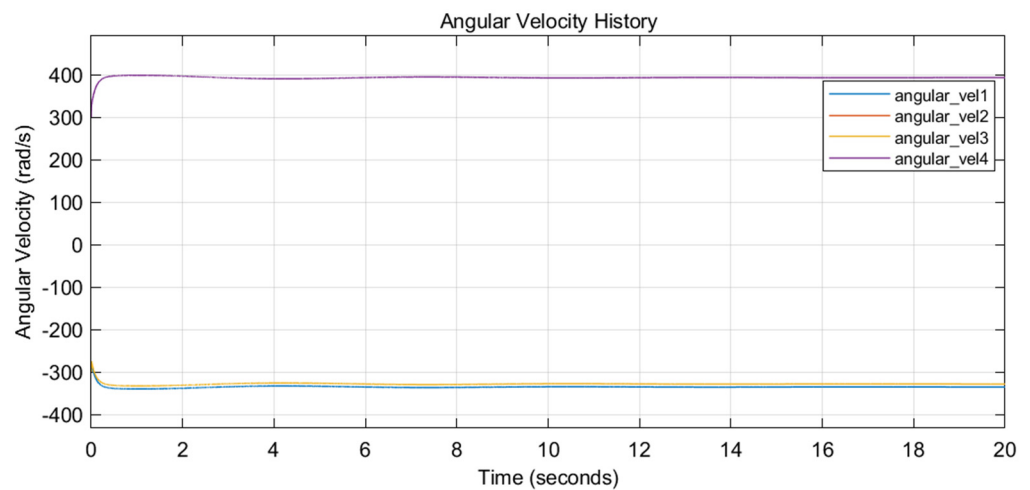**Figure 18.** Altitude history of Gait 2.

Figure 19. Angular velocity history of Gait 2.

6.2. Applicable Gait (Sufficient Conditions)

This section displays the applicability of each gait from Sections 5.1.1–5.1.4 (with five different (α_1, α_3) pairs in each section), determined via the method in (26).

Surprisingly, the resulting applicable values of (α_2, α_4) leading to stable results in each (α_1, α_3) in 20 (5×4) restrictions were highly similar. Except for one gait $((\alpha_1, \alpha_3) = (0.2, 0.4))$, which led to instability, the regions of applicable (α_2, α_4) for the remaining 19 cases contained the same triangular region governed by $(-1.3, 1.3)$, $(1.3, -1.3)$, and $(1, 1)$.
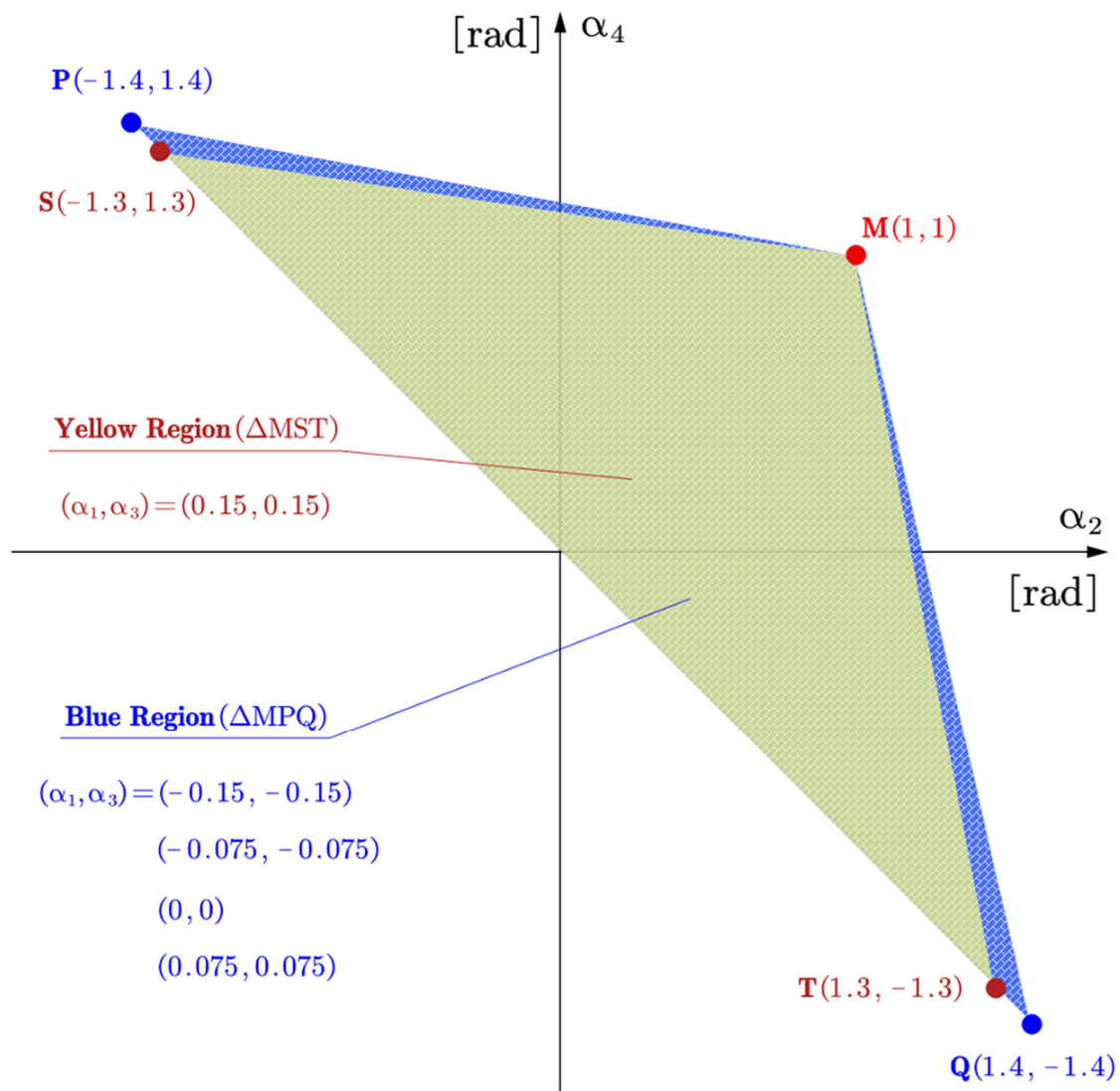

Figure 20. Admissible (α_2, α_4) when $\alpha_1 = \alpha_3$. M represents the gaits satisfying $\alpha_2 = \alpha_4 = 1$. P, S, T, Q represents the gaits satisfying $(\alpha_2, \alpha_4) = (-1.4, 1.4), (-1.3, 1.3), (1.3, -1.3), (1.4, -1.4)$, respectively.
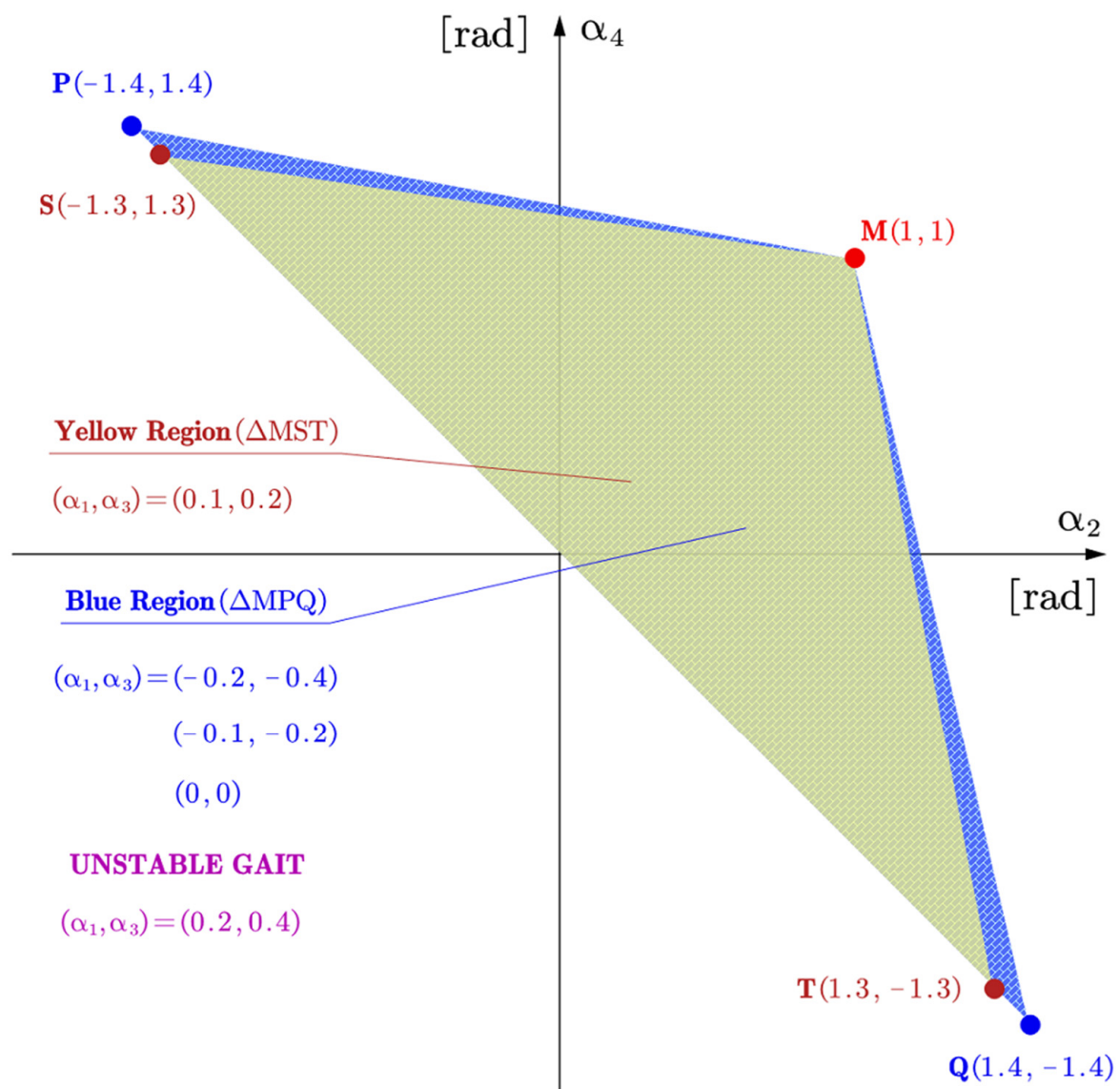
Figure 21. Admissible (α_2, α_4) when $\alpha_1 = \frac{1}{2}\alpha_3$. M represents the gaits satisfying $\alpha_2 = \alpha_4 = 1$. P, S, T, Q represent the gaits satisfying $(\alpha_2, \alpha_4) = (-1.4, 1.4), (-1.3, 1.3), (1.3, -1.3), (1.4, -1.4)$, respectively.
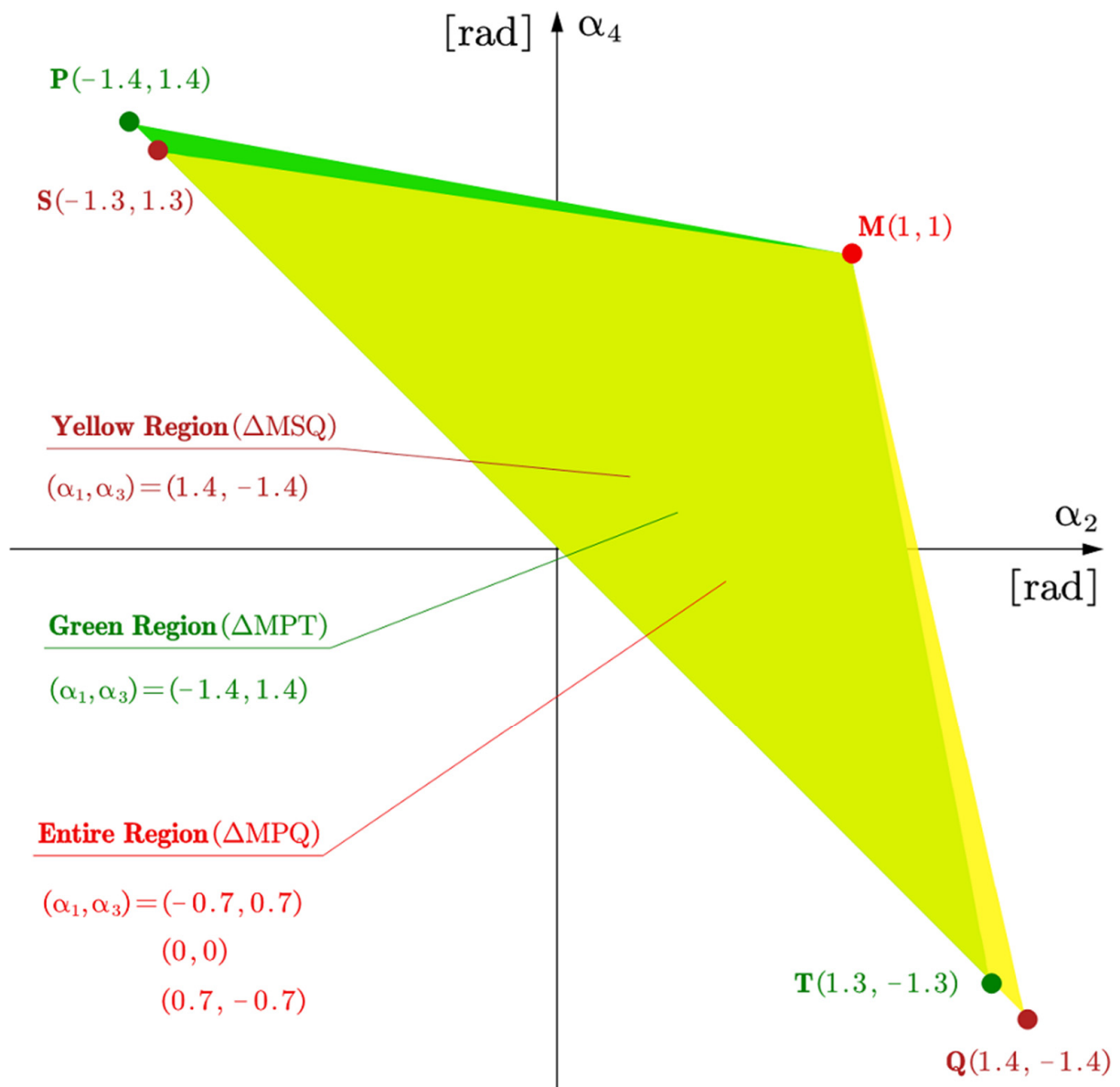
Figure 22. Admissible (α_2, α_4) when $\alpha_1 = -\alpha_3$. M represents the gaits satisfying $\alpha_2 = \alpha_4 = 1$. P, S, T, Q represent the gaits satisfying $(\alpha_2, \alpha_4) = (-1.4, 1.4), (-1.3, 1.3), (1.3, -1.3), (1.4, -1.4)$, respectively.

Figure 23. Admissible (α_2, α_4) when $\alpha_1 = -\frac{1}{2}\alpha_3$. M represents the gaits satisfying $\alpha_2 = \alpha_4 = 1$. P, S, T, Q represent the gaits satisfying $(\alpha_2, \alpha_4) = (-1.4, 1.4), (-1.3, 1.3), (1.3, -1.3), (1.4, -1.4)$, respectively.
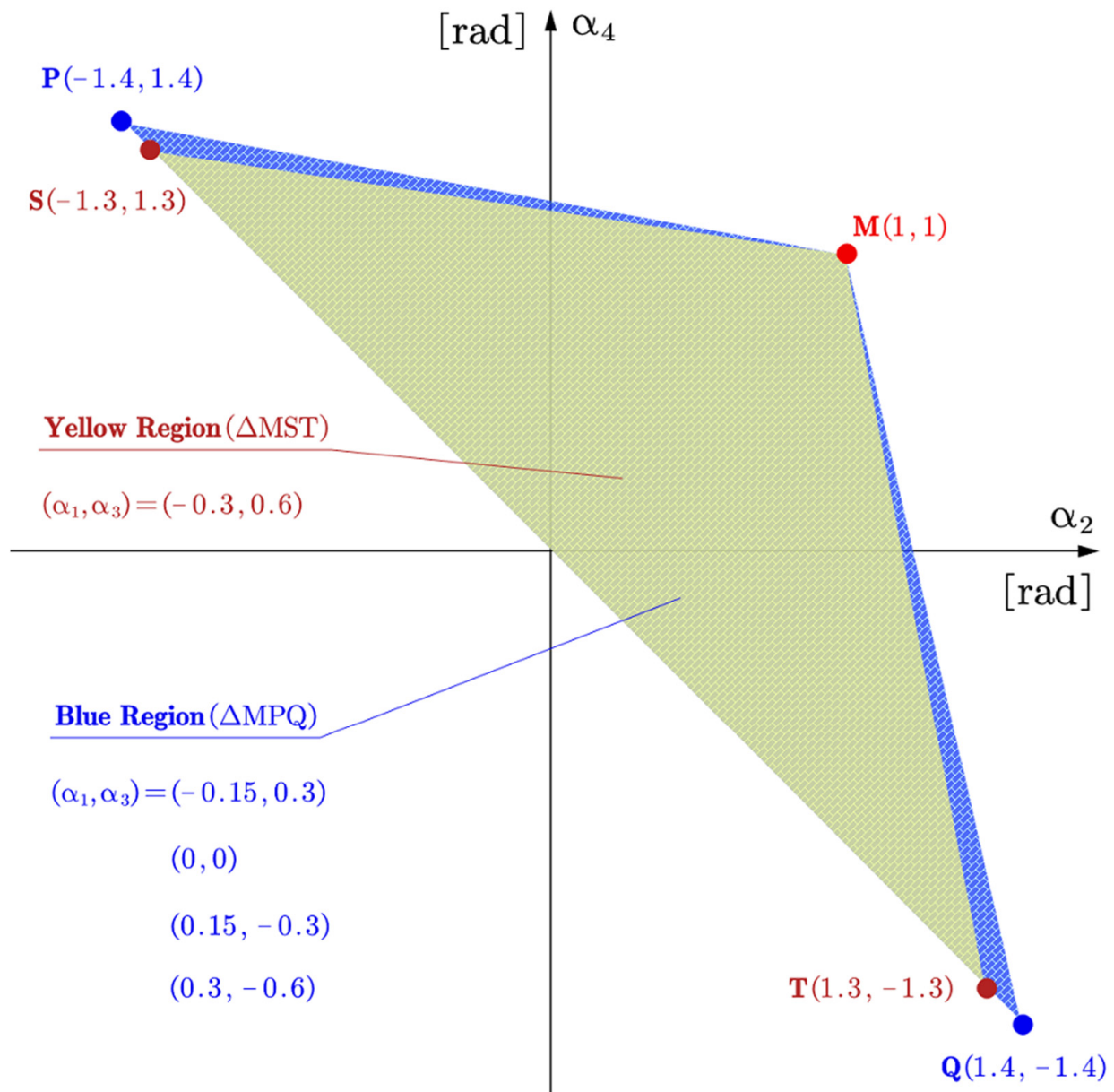
6.3. Over-Actuated Control

This section presents the control result for an over-actuated controller with eight control inputs, used to complete the same task with identical parameters and initial conditions. The attitude history, the altitude history, the angular velocities history of the propellers, and the tilting angles history are plotted in Figures 24–27, respectively.
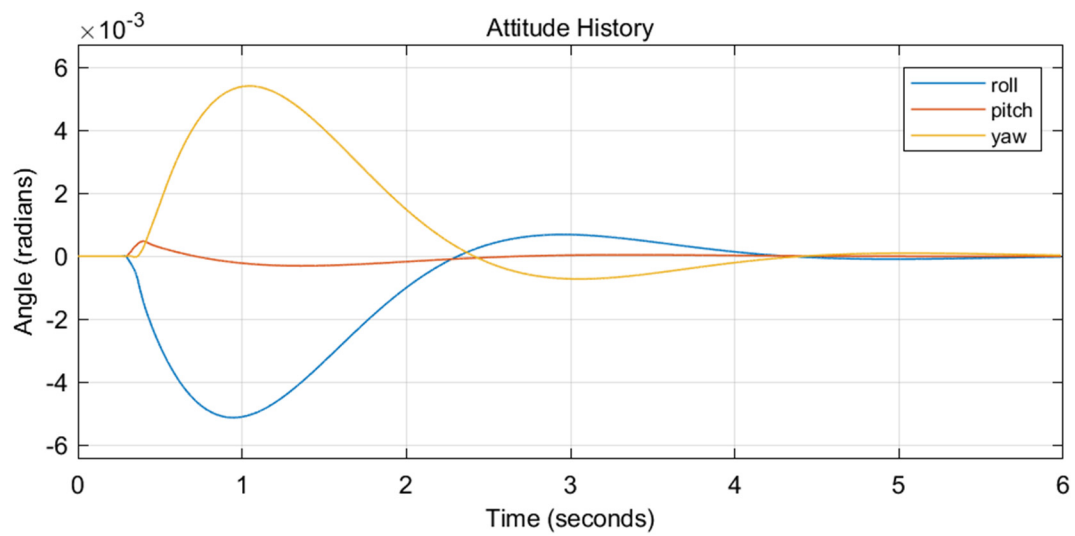
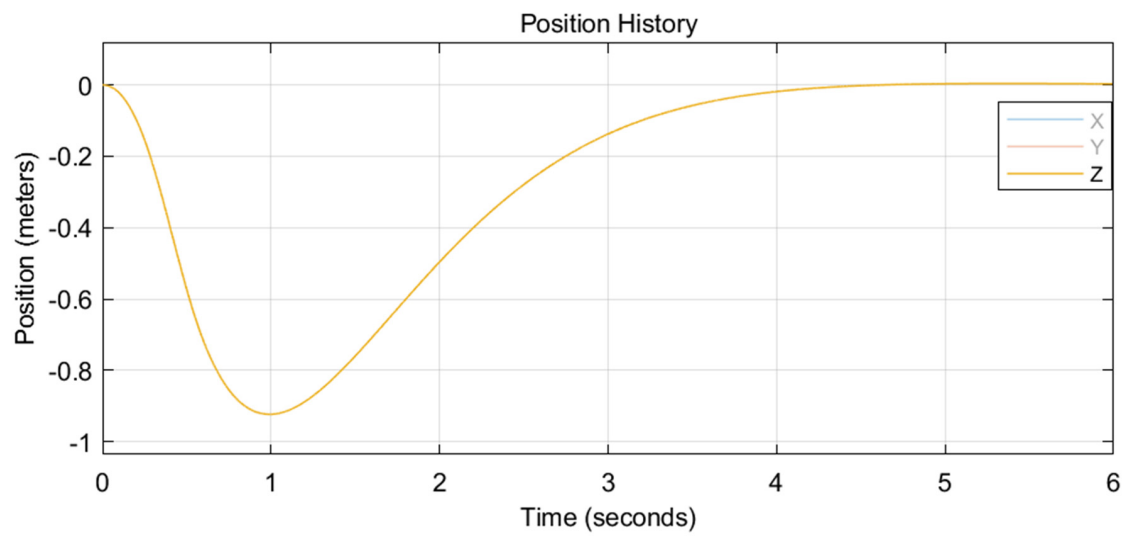**Figure 24.** Attitude history of over-actuated control.

Figure 25. Attitude history of over-actuated control.
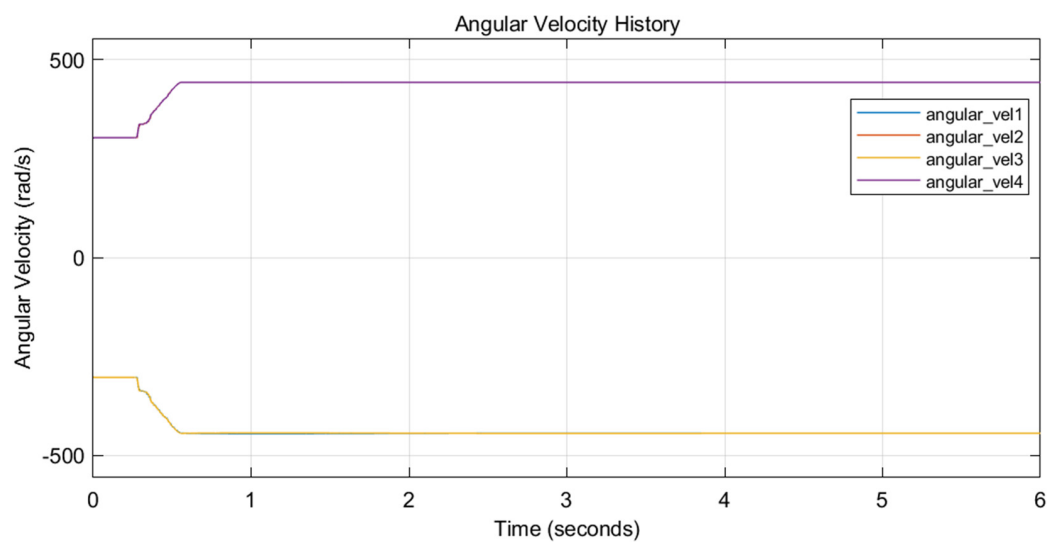

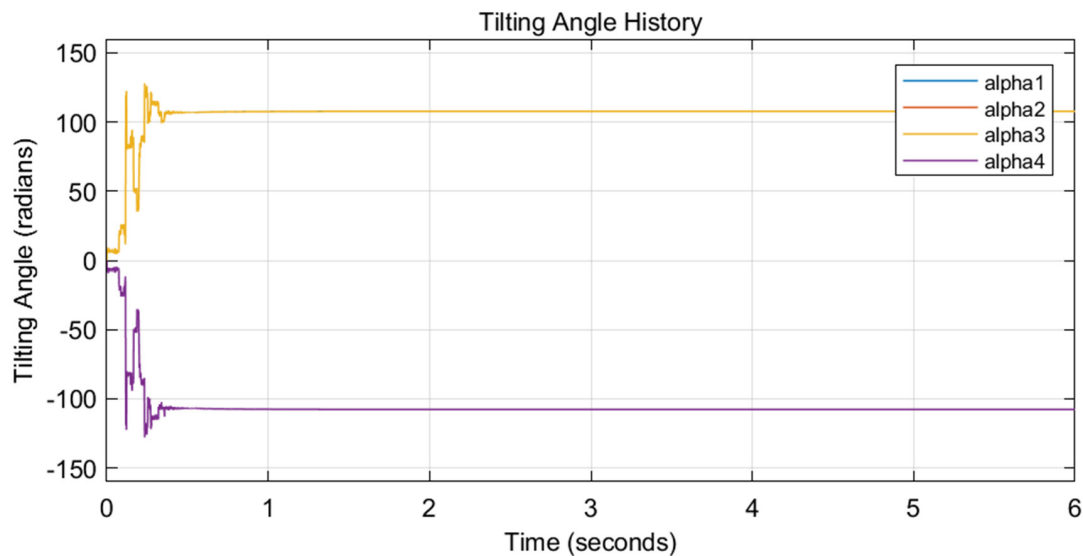**Figure 26.** Angular velocity history of over-actuated control.

Figure 27. Tilting angle history of over-actuated control.

Although the response was faster than in the control method proposed in this research, the tilting angles changed over-rapidly and intensively, which is commonly believed to be unrealistic.

7. Conclusions and Discussions

The necessary conditions to develop an invertible decoupling matrix for the attitude–altitude-based feedback linearization method have been determined and visualized for a tiltrotor.

For the gait restricted by $\alpha_1 = \alpha_3, \alpha_1 = \frac{1}{2} \cdot \alpha_3, \alpha_1 = -\alpha_3, \alpha_1 = -\frac{1}{2} \cdot \alpha_3$ within the specific region of interest given in (22), the feedback linearization had great success in terms of stabilization if, and only if, (α_2, α_4) lay inside the relevant region defined in Figures 20–23.

The angular velocities in each simulation that manifested a stable result avoided touching the non-negative constraints.

When the over-actuated controller was used for completing the same task, the tilting angle was maneuvered over-rapidly and intensively. In return, the tiltrotor received a faster response and less overshoot.

For the defined (α_1, α_3) of interest, the control result is very likely to be unstable if (α_2, α_4) lies outside the relevant colored areas in Figures 20–23.

These conclusions can offer effective guidance for designing the gait in a safe (invertible) region. For example, a different kind of feedback-linearization-based gait may allow (α_2, α_4) to lie within the triangular region governed by $(-1.3, 1.3)$, $(1.3, -1.3)$, and $(1, 1)$, because this region is most closely related to achieving a stable result.

The $\alpha_2 - \alpha_4$ planes (Figures 3, 5, 7 and 9) in Section 5.2 were divided into several regions by the invertibility-violating curves. We have argued that the applicable gait should lie in the same region. Furthermore, we asserted that crossing these curves is inevitable when switching from the gait in one region to the gait in another region. However, this is not always true.

It can be proven that the decoupling matrix for the gait $(\alpha_1, \alpha_2, \alpha_3, \alpha_4) = (0, 0, 0, 0)$ is always invertible, introducing no invertibility-violating curves. Thus, one may avoid crossing the invertibility-violating curves while switching the gait by adjusting (α_1, α_3) at the same time, e.g., the tiltrotor may return to the safe gait $(\alpha_1, \alpha_2, \alpha_3, \alpha_4) = (0, 0, 0, 0)$ as the middle step before switching to the desired gait. Further discussions are beyond the scope of this research.

Our next step is to develop a periodical gait for the tiltrotor in order to track a more complicated reference.

References

1.　Ryll, M.; Bülthoff, H.H.; Giordano, P.R. Modeling and Control of a Quadrotor UAV with Tilting Propellers. In Proceedings of the IEEE International Conference on Robotics and Automation, Saint Paul, MN, USA, 14–18 May 2012.

2.　Senkul, F.; Altug, E. Adaptive Control of a Tilt-Roll Rotor Quadrotor UAV. In Proceedings of the 2014 International Conference on Unmanned Aircraft Systems, ICUAS 2014, Orlando, FL, USA, 27–30 May 2014.

3.　Senkul, F.; Altug, E. Modeling and Control of a Novel Tilt-Roll Rotor Quadrotor UAV. In Proceedings of the 2013 International Conference on Unmanned Aircraft Systems, ICUAS 2013, Atlanta, GA, USA, 28–31 May 2013.

4.　Nemati, A.; Kumar, M. Modeling and Control of a Single Axis Tilting Quadcopter. In Proceedings of the American Control Conference, Portland, OR, USA, 4–6 June 2014.

5.　Bin Junaid, A.; De Cerio Sanchez, A.D.; Bosch, J.B.; Vitzilaios, N.; Zweiri, Y. Design and Implementation of a Dual-Axis Tilting Quadcopter. *Robotics* **2018**, *7*, 65. [CrossRef]

6.　Andrade, R.; Raffo, G.V.; Normey-Rico, J.E. Model Predictive Control of a Tilt-Rotor UAV for Load Transportation. In Proceedings of the 2016 European Control Conference, ECC 2016, Aalborg, Denmark, 29 June–1 July 2016.

7.　Nemati, A.; Kumar, R.; Kumar, M. Stabilizing and Control of Tilting-Rotor Quadcopter in Case of a Propeller Failure. In Proceedings of the ASME 2016 Dynamic Systems and Control Conference, DSCC 2016, Minneapolis, MN, USA, 12–14 October 2016; Volume 1.

8.　Anderson, R.B.; Marshall, J.A.; L'Afflitto, A. Constrained Robust Model Reference Adaptive Control of a Tilt-Rotor Quadcopter Pulling an Unmodeled Cart. *IEEE Trans. Aerosp. Electron. Syst.* **2021**, *57*, 39–54. [CrossRef]

9.　Badr, S.; Mehrez, O.; Kabeel, A.E. A Design Modification for a Quadrotor UAV: Modeling, Control and Implementation. *Adv. Robot.* **2019**, *33*, 13–32. [CrossRef]

10.　Bhargavapuri, M.; Patrikar, J.; Sahoo, S.R.; Kothari, M. A Low-Cost Tilt-Augmented Quadrotor Helicopter: Modeling and Control. In Proceedings of the 2018 International Conference on Unmanned Aircraft Systems, ICUAS 2018, Dallas, TX, USA, 12–15 June 2018.

11.　Badr, S.; Mehrez, O.; Kabeel, A.E. A Novel Modification for a Quadrotor Design. In Proceedings of the 2016 International Conference on Unmanned Aircraft Systems, ICUAS 2016, Arlington, VA, USA, 7–10 June 2016.

12.　Jiang, X.-Y.; Su, C.-L.; Xu, Y.-P.; Liu, K.; Shi, H.-Y.; Li, P. An Adaptive Backstepping Sliding Mode Method for Flight Attitude of Quadrotor UAVs. *J. Cent. South Univ.* **2018**, *25*, 616–631. [CrossRef]

13.　Jin, S.; Kim, J.; Kim, J.W.; Bae, J.H.; Bak, J.; Kim, J.; Seo, T.W. Back-Stepping Control Design for an Underwater Robot with Tilting Thrusters. In Proceedings of the 17th International Conference on Advanced Robotics, ICAR 2015, Istanbul, Turkey, 27–31 July 2015.

14.　Kadiyam, J.; Santhakumar, M.; Deshmukh, D.; Seo, T.W. Design and Implementation of Backstepping Controller for Tilting Thruster Underwater Robot. In Proceedings of the International Conference on Control, Automation and Systems, PyeongChang, Korea, 17–20 October 2018; Volume 2018.

15.　Scholz, G.; Popp, M.; Ruppelt, J.; Trommer, G.F. Model Independent Control of a Quadrotor with Tiltable Rotors. In Proceedings of the IEEE/ION Position, Location and Navigation Symposium, PLANS 2016, Savannah, GA, USA, 11–14 April 2016.

16.　Phong Nguyen, N.; Kim, W.; Moon, J. Observer-Based Super-Twisting Sliding Mode Control with Fuzzy Variable Gains and Its Application to Overactuated Quadrotors. In Proceedings of the IEEE Conference on Decision and Control, Miami, FL, USA, 17–19 December 2018; Volume 2018.

17.　Kumar, R.; Nemati, A.; Kumar, M.; Sharma, R.; Cohen, K.; Cazaurang, F. Tilting-Rotor Quadcopter for Aggressive Flight Maneuvers Using Differential Flatness Based Flight Controller. In Proceedings of the ASME 2017 Dynamic Systems and Control Conference, DSCC 2017, Tysons, VA, USA, 11–13 October 2017; Volume 3.

18.　Saif, A.-W.A. Feedback Linearization Control of Quadrotor with Tiltable Rotors under Wind Gusts. *Int. J. Adv. Appl. Sci.* **2017**, *4*, 150–159. [CrossRef]

19.　Offermann, A.; Castillo, P.; De Miras, J.D. Control of a PVTOL* with Tilting Rotors*. In Proceedings of the 2019 International Conference on Unmanned Aircraft Systems, ICUAS 2019, Atlanta, GA, USA, 11–14 June 2019.

20. Rajappa, S.; Bulthoff, H.H.; Odelga, M.; Stegagno, P. A Control Architecture for Physical Human-UAV Interaction with a Fully Actuated Hexarotor. In Proceedings of the IEEE International Conference on Intelligent Robots and Systems, Vancouver, BC, Canada, 24–28 September 2017; Volume 2017.

21. Scholz, G.; Trommer, G.F. Model Based Control of a Quadrotor with Tiltable Rotors. *Gyroscopy Navig.* **2016**, *7*, 72–81. [CrossRef]

22. Ryll, M.; Bülthoff, H.H.; Giordano, P.R. A Novel Overactuated Quadrotor Unmanned Aerial Vehicle: Modeling, Control, and Experimental Validation. *IEEE Trans. Control Syst. Technol.* **2015**, *23*, 540–556. [CrossRef]

23. Elfeky, M.; Elshafei, M.; Saif, A.W.A.; Al-Malki, M.F. Quadrotor Helicopter with Tilting Rotors: Modeling and Simulation. In Proceedings of the 2013 World Congress on Computer and Information Technology, WCCIT 2013, Sousse, Tunisia, 22–24 June 2013.

24. Park, S.; Lee, J.; Ahn, J.; Kim, M.; Her, J.; Yang, G.H.; Lee, D. ODAR: Aerial Manipulation Platform Enabling Omnidirectional Wrench Generation. *IEEE/ASME Trans. Mechatron.* **2018**, *23*, 1907–1918. [CrossRef]

25. Magariyama, T.; Abiko, S. Seamless 90-Degree Attitude Transition Flight of a Quad Tilt-Rotor UAV under Full Position Control. In Proceedings of the IEEE/ASME International Conference on Advanced Intelligent Mechatronics, AIM, Boston, MA, USA, 6–9 July 2020; Volume 2020.

26. Falanga, D.; Kleber, K.; Mintchev, S.; Floreano, D.; Scaramuzza, D. The Foldable Drone: A Morphing Quadrotor That Can Squeeze and Fly. *IEEE Robot. Autom. Lett.* **2019**, *4*, 209–216. [CrossRef]

27. Lu, D.; Xiong, C.; Zeng, Z.; Lian, L. Adaptive Dynamic Surface Control for a Hybrid Aerial Underwater Vehicle with Parametric Dynamics and Uncertainties. *IEEE J. Ocean. Eng.* **2020**, *45*, 740–758. [CrossRef]

28. Antonelli, G.; Cataldi, E.; Arrichiello, F.; Giordano, P.R.; Chiaverini, S.; Franchi, A. Adaptive Trajectory Tracking for Quadrotor MAVs in Presence of Parameter Uncertainties and External Disturbances. *IEEE Trans. Control Syst. Technol.* **2018**, *26*, 248–254. [CrossRef]

29. Lee, D.; Jin Kim, H.; Sastry, S. Feedback Linearization vs. Adaptive Sliding Mode Control for a Quadrotor Helicopter. *Int. J. Control Autom. Syst.* **2009**, *7*, 419–428. [CrossRef]

30. Al-Hiddabi, S.A. Quadrotor Control Using Feedback Linearization with Dynamic Extension. In Proceedings of the 2009 6th International Symposium on Mechatronics and its Applications, Sharjah, United Arab Emirates, 23–26 March 2009; pp. 1–3.

31. Mukherjee, P.; Waslander, S. Direct Adaptive Feedback Linearization for Quadrotor Control. In Proceedings of the AIAA Guidance, Navigation, and Control Conference, Minneapolis, MN, USA, 13–16 August 2012.

32. Rajappa, S.; Ryll, M.; Bulthoff, H.H.; Franchi, A. Modeling, Control and Design Optimization for a Fully-Actuated Hexarotor Aerial Vehicle with Tilted Propellers. In Proceedings of the IEEE International Conference on Robotics and Automation, Seattle, WA, USA, 26–30 May 2015; Volume 2015.

33. Dunham, W.; Petersen, C.; Kolmanovsky, I. Constrained Control for Soft Landing on an Asteroid with Gravity Model Uncertainty. In Proceedings of the American Control Conference, Boston, MA, USA, 6–8 July 2016; Volume 2016.

34. McDonough, K.; Kolmanovsky, I. Controller State and Reference Governors for Discrete-Time Linear Systems with Pointwise-in-Time State and Control Constraints. In Proceedings of the American Control Conference, Chicago, IL, USA, 1–3 July 2015; Volume 2015.

35. Kolmanovsky, I.; Kalabić, U.; Gilbert, E. Developments in Constrained Control Using Reference Governors. *IFAC Proc.* **2012**, *4*, 282–290. [CrossRef]

36. Bemporad, A. Reference Governor for Constrained Nonlinear Systems. *IEEE Trans. Autom. Control* **1998**, *43*, 415–419. [CrossRef]

37. Shen, Z.; Ma, Y.; Tsuchiya, T. Stability Analysis of a Feedback-Linearization-Based Controller with Saturation: A Tilt Vehicle with the Penguin-Inspired Gait Plan. *arXiv* **2021**, arXiv:2111.14456.

38. Franchi, A.; Carli, R.; Bicego, D.; Ryll, M. Full-Pose Tracking Control for Aerial Robotic Systems with Laterally Bounded Input Force. *IEEE Trans. Robot.* **2018**, *34*, 534–541. [CrossRef]

39. Horla, D.; Hamandi, M.; Giernacki, W.; Franchi, A. Optimal Tuning of the Lateral-Dynamics Parameters for Aerial Vehicles with Bounded Lateral Force. *IEEE Robot. Autom. Lett.* **2021**, *6*, 3949–3955. [CrossRef]

40. Shen, Z.; Tsuchiya, T. State Drift and Gait Plan in Feedback Linearization Control of A Tilt Vehicle. *arXiv* **2021**, arXiv:2111.04307.

41. Chernova, S.; Veloso, M. An Evolutionary Approach to Gait Learning for Four-Legged Robots. In Proceedings of the 2004 IEEE/RSJ International Conference on Intelligent Robots and Systems (IROS), Sendai, Japan, 28 September–2 October 2004; Volume 3.

42. Bennani, M.; Giri, F. Dynamic Modelling of a Four-Legged Robot. *J. Intell. Robot. Syst. Theory Appl.* **1996**, *17*, 419–428. [CrossRef]

43. Talebi, S.; Poulakakis, I.; Papadopoulos, E.; Buehler, M. Quadruped Robot Running with a Bounding Gait. In *Experimental Robotics VII*; Rus, D., Singh, S., Eds.; Springer: Berlin/Heidelberg, Germany, 2007.

44. Lewis, M.A.; Bekey, G.A. Gait Adaptation in a Quadruped Robot. *Auton. Robot.* **2002**, *12*, 301–312. [CrossRef]

45. Hirose, S. A Study of Design and Control of a Quadruped Walking Vehicle. *Int. J. Robot. Res.* **1984**, *3*, 113–133. [CrossRef]

46. Luukkonen, T. Modelling and Control of Quadcopter. *Indep. Res. Proj. Appl. Math.* **2011**, *22*, 22.

47. Goodarzi, F.A.; Lee, D.; Lee, T. Geometric Adaptive Tracking Control of a Quadrotor Unmanned Aerial Vehicle on SE(3) for Agile Maneuvers. *J. Dyn. Syst. Meas. Control* **2015**, *137*, 091007. [CrossRef]

48. Shi, X.-N.; Zhang, Y.-A.; Zhou, D. A Geometric Approach for Quadrotor Trajectory Tracking Control. *Int. J. Control* **2015**, *88*, 2217–2227. [CrossRef]

49. Lee, T.; Leok, M.; McClamroch, N.H. Nonlinear Robust Tracking Control of a Quadrotor UAV on SE(3): Nonlinear Robust Tracking Control of a Quadrotor UAV. *Asian J. Control* **2013**, *15*, 391–408. [CrossRef]

50. Shen, Z.; Tsuchiya, T. Singular Zone in Quadrotor Yaw-Position Feedback Linearization. *arXiv* **2021**, arXiv:2110.07179.
51. Mistier, V.; Benallegue, A.; M'Sirdi, N.K. Exact Linearization and Noninteracting Control of a 4 Rotors Helicopter via Dynamic Feedback. In Proceedings of the IEEE International Workshop on Robot and Human Interactive Communication, Paris, France, 18–21 September 2001; pp. 586–593.
52. Das, A.; Subbarao, K.; Lewis, F. Dynamic Inversion with Zero-Dynamics Stabilisation for Quadrotor Control. *IET Control Theory Appl.* **2009**, *3*, 303–314. [CrossRef]